

To appear in the Astrophysical Journal

Constraining the Lifetime of Circumstellar Disks in the Terrestrial Planet Zone: A Mid-IR Survey of the 30-Myr-old Tucana-Horologium Association

Eric E. Mamajek, Michael R. Meyer, Philip M. Hinz, William F. Hoffmann

*Steward Observatory, Department of Astronomy, The University of Arizona,
933 N. Cherry Ave., Tucson, AZ 85721*

Martin Cohen

*Radio Astronomy Laboratory, 601 Campbell Hall, University of California at Berkeley,
Berkeley, CA 94720*

Joseph L. Hora

*Harvard-Smithsonian Center for Astrophysics,
60 Garden St., MS-65, Cambridge, MA 02138*

eem@as.arizona.edu

ABSTRACT

We have conducted an N-band survey of 14 young stars in the ~ 30 Myr-old Tucana-Horologium Association to search for evidence of warm, circumstellar dust disks. Using the MIRAC-BLINC camera on the Magellan I (Baade) 6.5-m telescope, we find that none of the stars have a statistically significant N-band excess compared to the predicted stellar photospheric flux. Using three different sets of assumptions, this null result rules out the existence of the following around these post-T Tauri stars: (a) optically-thick disks with inner hole radii of $\lesssim 0.1$ AU, (b) optically-thin disks with masses of $> 10^{-6} M_{\oplus}$ (in $\sim 1\text{-}\mu\text{m}$ -sized grains) within $\lesssim 10$ AU of these stars, (c) scaled-up analogs of the solar system zodiacal dust cloud with $> 4000\times$ the emitting area. Our survey was sensitive to dust disks in the terrestrial planet zone with fractional luminosity of $\log(L_{\text{dust}}/L_{*}) \sim 10^{-2.9}$, yet none were found. Combined with results from previous surveys, these data suggest that circumstellar dust disks become so optically-thin as to be undetectable at N-band before age ~ 20 Myr. We also present N-band photometry for several members of other young associations and a subsample of targets

that will be observed with *Spitzer Space Telescope* by the *Formation and Evolution of Planetary Systems* (FEPS) Legacy Science Program. Lastly, we present an absolute calibration of MIRAC-BLINC for four filters (L , N , 11.6, and Q_s) on the Cohen-Walker-Witteborn system.

Subject headings: — circumstellar matter — infrared: stars — galaxy : open clusters and associations: individual (Tucana-Horologium Association) — planetary systems: formation — planetary systems: protoplanetary disks

1. INTRODUCTION

Circumstellar disks appear to be a nearly ubiquitous by-product of the star-formation process. Most low-mass stars in the youngest star-formation regions (e.g. the ~ 1 -Myr-old Orion Nebula Cluster) have spectroscopic or photometric evidence of a circumstellar disk (Hillenbrand et al. 1998). The masses of circumstellar disks found around some T Tauri stars are similar to that of the minimum mass solar nebula (Beckwith et al. 1990). Their physical sizes are similar to that of our own solar system (10s-100s AU; McCaughrean & O’Dell 1996). Considering their masses, dimensions, and appearance at the very earliest stages of stellar evolution, these disks are considered “protoplanetary”. Radial velocity surveys of nearby solar-type stars indicate that at least $\sim 5\%$ have at least one Jupiter-mass planet orbiting within a few AU (Marcy & Butler 2000), indicating that the formation of gas giant planets is one likely outcome of circumstellar disk evolution.

The incidence of inner protoplanetary accretion disks diminishes with age, being very common at ages < 1 Myr, and very rare at > 10 Myr. The fraction of low-mass stars with disks inferred by IR excess (in the L-band; $3.5\ \mu\text{m}$) diminishes with age, with half losing their inner disks ($\lesssim 0.1$ AU) by age ~ 3 Myr (e.g. Haisch, Lada, & Lada 2001a). Using population statistics of pre-MS stars in the Taurus molecular clouds, multiple studies have demonstrated that the transition time for disks inside of ~ 1 AU to go from optically-thick to optically-thin is $\sim 10^5$ yr (Skrutskie et al. 1990; Wolk & Walter 1996). While some studies argue that accretion terminates by age ~ 6 Myr (Haisch, Lada, & Lada 2001a), recent studies suggest that it may continue at lower accretion rates around some stars until at least age ~ 10 Myr (Muzerolle et al. 2000; Mamajek, Meyer, & Liebert 2002; Lawson et al. 2002; Lawson, Lyo, & Muzerolle 2004). There are preliminary indications that disks may persist longer for stars in associations which lack massive OB stars and for the lowest mass stars (e.g. Lyo et al. 2003; Haisch, Lada, & Lada 2001b). Although understanding the evolution of accretion disks has improved, the evolution of dust in the terrestrial planet zone is still largely unexplored.

Although the phenomenon of optically-thick accretion disks appears to be isolated to the first \sim few Myr of a star’s life, numerous examples of older stars with optically-thin dust disks have been found over the past two decades, primarily using space-based IR telescopes, e.g. *InfraRed Astronomical Satellite* (IRAS) and *Infrared Space Observatory* (ISO) (Backman & Paresce 1993; Lagrange, Backman, & Artymowicz 2000). Optically-thin disks have been found around stars over a wide range of ages and masses, but those with the highest fractional luminosity ($f_d = L_{\text{disk}}/L_\star$) are mostly confined to those younger than $<\text{few} \times 100$ Myr in age (Habing et al. 2001; Spangler et al. 2001). These dusty “debris” disks are inferred to be created by the collisions of larger bodies, rather than primordial ISM dust (Harper, Loewenstein, & Davidson 1984; Backman & Paresce 1993). For micron-size dust grains orbiting between ~ 0.1 -10 AU, the timescale for Poynting-Robertson drag to pull the grains into the star ($\sim 10^{1-5}$ yr) is short compared to typical stellar ages ($\sim 10^{7-10}$ yr), implying that either the observed phenomena is short-lived, or that grains must be replenished through collisions of larger bodies. There is preliminary evidence for a monotonic decrease in dust disk optical depth with age (Spangler et al. 2001), or possibly a more precipitous drop in optical depth after age ~ 400 Myr (Habing et al. 2001). Most of the known debris disks have been identified by excess far-IR emission above that of the stellar photosphere (e.g. Silverstone 2000), with characteristic dust temperatures of ~ 30 -100 K. Despite efforts to find warm ($T \sim 200$ -300 K) dust disks around field stars, precious few examples with detectable 10 - $12\mu\text{m}$ excesses are known (Aumann & Probst 1991).

Observational constraints on the evolution of circumstellar dust in the terrestrial planet zone are currently scarce. Planned observations with the recently launched *Spitzer Space Telescope* (SST) by the *Formation and Evolution of Planetary Systems* (FEPS) Legacy Science program¹, among others, will remedy this situation. FEPS plans to systematically trace the evolution of circumstellar gas and dust around sun-like stars between the epoch of optically-thick accretion disks (ages \sim few Myr) to the epoch of mature planetary systems (ages \sim few Gyr; Meyer et al. 2002, 2004).

Although SST promises to provide a leap in our understanding of the circumstellar environs of stars, we can address a basic question about disk evolution using currently available ground-based facilities. *How much dust remains within a few AU of young stars during the epoch of terrestrial planet formation?* We address this question through a mid-IR survey of a sample of young, low-mass stars with ages of ~ 30 Myr: the Tuc-Hor Association.

Dynamical simulations suggest that, given the surface mass density of the minimum-mass solar nebula, runaway growth can take place and form Moon-sized planetary “em-

¹<http://feeps.as.arizona.edu>

bryos” within $\sim 10^5$ yr (Wetherill & Stewart 1993). When the largest embryos reach radii of ~ 1000 km, gravitational interactions increase the eccentricities and collision velocities of smaller planetesimals, causing more dust-producing collisions (Kenyon & Bromley 2004). Over the next $\sim 10^7$ - 10^8 yr, the growth of the largest embryos is dominated by giant impacts, which consolidate the embryos into a small number of terrestrial planets (Agnor, Canup, & Levison 1999; Chambers 2001). During this epoch in our own solar system, the proto-Earth is hypothesized to have been impacted by a Mars-sized planetesimal, which formed the Earth-Moon system (Hartmann & Davis 1975; Stevenson 1987). Chronometry studies using radioactive parent-daughter systems (such as ^{182}Hf - ^{182}W) suggest that the Earth-Moon impact occurred 25-35 Myr after the formation of the solar system (Kleine et al. 2002; Kleine, Mezger, & Münker 2003). We know that around at least one star (our Sun), terrestrial planets were forming at age ~ 30 Myr.

In §2 we describe the sample, our mid-IR observations, and data reduction. §3 presents the results of our photometry. We present three simple circumstellar disk models in §4, and calculate upper limits to the amount of dust orbiting within $\lesssim 10$ AU of the stars observed. In §5 we discuss our results in light of previous observational and theoretical efforts in order to better understand disk evolution around young stars. In the Appendix, we present information related to the photometric calibration of the MIRAC-BLINC system, as well as details regarding stars for which mid-IR excesses were detected.

2. OBSERVATIONS

2.1. The Sample

Our mid-IR survey contains 14 low-mass stars that we argue are probable members of the ~ 30 -Myr-old Tuc-Hor Association. The observations of the Tuc-Hor stars are presented in Table 2. Observations of some Tuc-Hor candidates that we reject as members, and other young stars (some of which are FEPS SST Legacy Science targets) are included in Table 3. Here we discuss some technical aspects of the Tuc-Hor sample.

The Tucana and Horologium associations are young stellar moving groups that were identified nearly contemporaneously by Zuckerman & Webb (2000, ZW00) and Torres et al. (2000, TDQ00). Zuckerman, Song, & Webb (2001, ZSW01) present an updated membership list and photometry, and suggest that the similar ages, kinematics, and positions of the Tucana and Horologium associations allow us to consider them a single group (“Tuc-Hor”). We adopt ~ 30 Myr as a reasonable age estimate for Tuc-Hor based on recent values in the literature (see Table 1).

The published membership lists for Tuc-Hor appear to be somewhat subjective and contain some stars that are unlikely to be members. In order to include stars that are plausibly members of Tuc-Hor as part of our study, we used kinematics as the primary membership criterion (in addition to the other criteria used in previous studies). For the combined Tuc-Hor membership lists of TDQ00, ZW00, ZSW01, we calculate membership probabilities using the equations of de Bruijne (1999), the heliocentric space motion of the Tucana nucleus from ZW00, and the best long-baseline proper motions available at present (preferably Tycho-2 or UCAC2; Høg et al. 2000; Zacharias et al. 2003). We reserve rigorous discussion of membership and kinematics for a separate future study. For this study, we retain only those stars whose membership we could not reject based on proper motion data. We find that $\sim 30\%$ of the stars proposed as members of Tuc-Hor have proper motions inconsistent with the motion of the assumed Tucana “nucleus” (centered on the β Tuc mini-cluster; using space motion vector given by Zuckerman & Webb 2000). The published membership lists appear to contain several field stars, a handful of which we observed with MIRAC (Table 3) before appreciating that they were probable non-members. Care should be used by investigators employing samples of recently-discovered, diffuse stellar associations (e.g. Tuc-Hor) for the study of age-dependent stellar phenomena.

We include in our Tuc-Hor sample the active dwarf HD 105 (= HIP 490). HD 105 is in the same region of sky ($\alpha, \delta(\text{ICRS}) = 00^h05^m, -41^\circ45'$) as the other proposed Tuc-Hor stars, and has a Hipparcos distance of $d = 40$ pc. For our calculations we adopt the long baseline Tycho-2 proper motion (Høg et al. 2000) and the Tuc-Hor space motion vector from Zuckerman & Webb (2000). In subjecting HD 105 to the same kinematic tests as the other Tuc-Hor candidates, we are unable to reject its membership. The calculated cluster parallax (25.3 mas) and predicted radial velocity (0 km s^{-1}) agree very well with the observed trigonometric parallax ($24.9 \pm 0.9 \text{ mas}$; ESA 1997) and measured RV ($+1.7 \pm 2.5 \text{ km s}^{-1}$; Wichmann, Schmitt, & Hubrig 2003). The equivalent width of the Li I $\lambda 6707$ line (165 mÅ; Cutispoto et al. 2002) is similar to that for early-G-type members of ~ 50 Myr-old IC 2602 and IC 2391 clusters (Randich et al. 2001), and stronger than that found in ~ 120 -Myr-old Pleiades stars (Soderblom et al. 1993). Finally, the X-ray luminosity of HD 105 ($\log(L_X) = 29.4 \text{ erg s}^{-1}$; Cutispoto et al. 2002) is similar to what is expected for early-G stars with ages of 10-100 Myr (Briceño et al. 1997). Therefore, we conclude that HD 105 is a likely member of the Tuc-Hor association.

2.2. Data Acquisition

Mid-IR images of the Tuc-Hor members and other young stars were obtained during the nights of 6-10 August 2001 and 22 August 2002 (UT) with the MIRAC-BLINC instrument on the Magellan I (Baade) 6.5-m alt-az telescope at Las Campanas Observatory, Chile. The *Mid-InfraRed Array Camera* (MIRAC-3) contains a Rockwell HF16 128×128 hybrid BIB Si:As array, and was built at the Steward Observatory, University of Arizona, and the Harvard-Smithsonian Center for Astrophysics (Hoffmann et al. 1998). The *Bracewell Infrared Nulling Cryostat* (BLINC) is a nulling interferometer mated to MIRAC-3 (Hinz et al. 2000). In our observing mode, however, BLINC is used as a re-imaging system, reducing the f/11 beam from the Magellan tertiary mirror to a f/20 beam required for the MIRAC-3 instrument. The pixel scale is $0.123''/\text{pixel}$, resulting in a FOV of $15.7''$.

Our intent was to survey for circumstellar dust surrounding our target stars in the terrestrial planet zone ($\sim 0.3\text{-}3\text{ AU}$), with characteristic temperatures of $\sim 300\text{ K}$, and corresponding Wien emission peak at $\sim 10\text{ }\mu\text{m}$. Observations were obtained with either the wide-band N filter ($\lambda_{iso} = 10.34\text{ }\mu\text{m}$ for an A0 star, where λ_{iso} is the isophotal wavelength, e.g. Golay 1974) or narrow-band “11.6” filter ($\lambda_{iso} = 11.57\text{ }\mu\text{m}$ for an A0 star) in standard chop-nod mode (4 position beam switching; see Appendix 1 of Hoffmann & Hora 1999). The nod and chop separations were $8''$, and the chop (frequency of 3-10 Hz) was in a direction perpendicular to the nod vector. The chop-nod imaging technique produces two positive and two negative images of the star in a square configuration on the detector. The nod separation was chosen so that all four images of the star appear on the detector with sufficient room for determination of the background flux in annuli surrounding each star image. We found that using chop frequencies between 3 and 10 Hz mitigated the effects of poorly subtracted sky background (background noise increases as chop frequency decreases) while maintaining observing efficiency (increasing the chop frequency adds overhead time, with minimal improvement in background subtraction). Chopping was done with an internal pupil plane beam-switching mirror within BLINC. The frame time (on-chip integration time) was either 10 ms (N -band) or 40 ms (11.6-band), and these frames were co-added in 15-30 s long integrations per nod beam. We found that derotating the MIRAC-BLINC instrument (i.e. freezing the cardinal sky directions on the detector) in the Nasmyth port during observations resulted in poorer background subtraction compared to turning the derotation off. Hence, for the majority of observations taken during these nights, the instrument derotation was turned off. The ability to guide the telescope while derotating the instrument, was not available during our observing runs. Hence the telescope was not guiding during most of our observations. This had negligible impact on the achieved image quality, but limited our ability to reliably co-add data for faint sources.

2.3. Reduction

The MIRAC images were reduced using the custom program *mrc2fts* (Hora 1991) and IRAF² routines. Flat fields were constructed from images of high (dome) and low (sky) emissivity surfaces. A median sky frame was produced and subtracted from the individual ($N \simeq 10$) dome frames. The results were then median combined to produce the final flat field. The pixel-to-pixel variation in sensitivity ($\sim 2\%$ r.m.s.) of the MIRAC detector is small enough that flat-fielding had negligible effect on our derived photometry.

Aperture photometry was derived using the IRAF *phot* package. We used aperture radii of either $0.62''$ (5 px) or $1.23''$ (10 px), depending on which flux had the higher S/N ratio after the photometric errors were fully propagated (dominated by sky noise for large aperture or uncertainty in aperture correction for smaller apertures). The photometry derived with aperture radii of 5 px and 10 px were consistent within the errors for all of the stars observed. The background level was determined by measuring the mean sky value per pixel in an annulus centered on the star with inner radius $1.85''$ (15 pix) and outer radius $3.08''$ (25 pix) for subtraction. The background annulus radii were chosen so as to sample a negligible contribution of the star’s PSF, but to avoid the PSFs from the other images of the same star. For the faintest sources, an aperture radius of 5 px was usually used, in which case an aperture correction was applied to place all photometry on the 10 px system. The aperture corrections were determined nightly using standard stars, and the typical correction to the 5 px aperture radius photometry was -0.32 ± 0.05 mag. Photometric solutions (zero points and airmass corrections) were determined for every night of observations. The typical airmass corrections at N -band were 0.1 - 0.2 mag airmass⁻¹. The conversion between fluxes (in mJy) and magnitudes is simply $mag_{\lambda}(\text{star}) = -2.5 \log\{f_{\lambda}(\text{star})/f_{\lambda}(0)\}$, where $f_{\lambda}(\text{star})$ is the star’s flux at wavelength λ , and $f_{\lambda}(0)$ is the flux of a zero-magnitude star (see Appendix A). The sensitivity was such that we could detect a star with of magnitude 7.5 in N -band, at $S/N \simeq 5$, with 600 s of on-source integration time.

We observed standard stars taken from the MIRAC manual (Hoffmann & Hora 1999), the list of ESO IR standards (van der Blik, Manfroid, & Bouchet 1996), and the list of Cohen et al. (1999). M. C. calculated an independent calibration of the MIRAC photometric system, using the approach identical to that described in Cohen, Wheaton, & Megeath (2003). Discussion on the input data for the absolute photometric calibration, the zero-magnitude attributes of the MIRAC filter systems, and standard star fluxes, are given in

²IRAF is distributed by the National Optical Astronomy Observatories, which are operated by the Association of Universities for Research in Astronomy, Inc., under cooperative agreement with the National Science Foundation. <http://iraf.noao.edu>

Appendix A. The absolute accuracy of the standard star fluxes among the four filters ranges from 1.7-4.5%.

3. RESULTS

N -band photometry for young stars in Tuc-Hor is presented in Table 4, while photometry for stars in other regions (most belonging to young, nearby associations) is presented in Table 5. Near-infrared (JHK_s) photometry from the 2MASS catalog (Cutri et al. 2003) was used to help predict the brightness of the stellar photospheres at $10\mu\text{m}$. For the range of spectral types investigated, models predict that $([11.6] - N) \simeq 0.00$ within our photometric errors (typically ~ 0.05 - 0.10 mag), hence we plot $(K_s - N)$ and $(K_s - [11.6])$ on the same color-color plot, and generically refer to these colors as “ $(K_s - N)$ ” throughout. A color-color plot of the Tuc-Hor stars is illustrated in Fig. 1.

Fig. 1 indicates that $(K_s - N)$ colors are fairly uniform for stars with $(J - K_s) < 0.7$, i.e. for FGK stars. We decided to analyze the M stars separately from the FGK stars. We surmise that much of the structure in the published color-color relations for dwarfs is probably due to statistical fluctuations (e.g. Cohen et al. 1987; Waters, Cote, & Aumann 1987; Mathioudakis & Doyle 1993; Kenyon & Hartmann 1995). After examining our data and those from previous studies of large dwarf samples, we decided to assume a constant $(K_s - N)$ color for the photospheres of FGK stars. In calculating a mean intrinsic $(K_s - N)$ color, we include the FGK stars in Tables 4 and 5, but exclude the FGK stars HD 143006, [PZ99] J161411 (both with $(K_s - N) \simeq 2$), and HIP 95270 and HIP 99273 (known to have far-IR excesses which may contaminate N -band flux, e.g. Zuckerman & Song 2004). The median, unweighted mean, and weighted mean $(K_s - N)$ color for the FGK stars are all similar (0.05 , 0.04 ± 0.02 , and 0.07 ± 0.02 , respectively). These estimates agree well with the mean FGK dwarf color found by Fajardo-Acosta, Beichman, & Cutri (2000, $(K_s - [12]) \simeq +0.04$ implies $(K_s - N) \simeq +0.05$) and are close to the value for AFGK-type dwarfs found by Aumann & Probst (1991, $(K_{CIT} - [12]) = +0.02$ implying $(K_s - N) = +0.01$)³. Within the uncertainties, *our measured mean $(K_s - N)$ color for FGK dwarfs is consistent with previous determinations. The mean colors for the young stars in our observing program do not appear to be biased toward red $(K_s - N)$ colors due to the presence of circumstellar material.* We adopt $(K_s - N)_{\text{phot}} = +0.05$ as the photospheric color for FGK-type stars with

³Although not explicitly stated, the K photometry from Aumann & Probst (1991) appears to be on the CIT system, where 2MASS $K_s = K_{CIT} - 0.019$ (Carpenter 2001). The MIRAC N -band photometric system assumes $N = 0.00$ for Vega, whereas Aumann & Probst (1991) list $[12] = +0.01$ for Vega. We ignore any color terms in converting $[12]$ to a predicted N magnitude, and derive $(K_s - N) \simeq (K_{CIT} - [12]) - 0.01$.

$$(J - K_s) < 0.69.$$

The observed $(K_s - N)$ colors of the M-type stars are systematically redder than those of the FGK stars, as well as the M-giant standards. We looked for independent confirmation that the turn-up in $(K_s - N)$ color for the coolest dwarfs is a real effect, and not due to circumstellar material. We measure a color of $(K_s - [11.6]) = 0.33 \pm 0.06$ for the ~ 12 -Myr-old M0 star GJ 803. Song et al. (2002) studied the spectral energy distribution of GJ 803 and concluded that the observed cold dust excess detected by IRAS at $60\mu\text{m}$ does not contribute significant flux at $12\mu\text{m}$, and that the IRAS $12\mu\text{m}$ flux is consistent with a NextGen model photosphere. Our observed $11.6\mu\text{m}$ flux (608 ± 32 mJy) agrees very well with the predicted photospheric flux (633 mJy at $11.6\mu\text{m}$), as well as the color-corrected IRAS $12\mu\text{m}$ flux (537 ± 32 mJy). These observations confirm that the observed $(K_s - [11.6])$ color for GJ 803 is photospheric, and that the turn-up in $(K_s - N)$ color for M stars is real. It appears that none of the M-type stars has a statistically significant mid-IR excess. For the purposes of calculating upper limits on mid-IR excess, we fit a line to the mean $(K_s - N)$ colors for the KM-type stars with $(J - K_s) > 0.6$ (excluding the T Tauri star [PZ99] J161411), and model the M-type dwarf photosphere colors as: $(K_s - N)_{phot} = -0.947 + 1.448 \times (J - K_s)$ ($0.69 < (J - K_s) < 0.92$).

We determine whether a star has detectable excess at N or 11.6 through calculating the excess as:

$$E(N) = N - N_{phot} = N - K_s + (K_s - N)_{phot} \quad (1)$$

$$\sigma^2[E(N)] = \sigma^2[N] + \sigma^2[K_s] + \sigma^2[(K_s - N)_{phot}] \quad (2)$$

The contribution to the N -band excess from interstellar extinction will only become similar in size to our photometric errors if $A_V \gtrsim 1\text{-}2$ mag, hence we can safely ignore extinction for the stars observed. We examined the residuals (defined as $E(N)/\sigma[E(N)]$) in order to identify statistically-significant outliers (i.e. possible N -band excess stars). The ~ 5 -Myr-old Upper Sco members HD 143006 and [PZ99] J161411 (Preibisch & Zinnecker 1999) both stand out with definite N -band excesses ($\simeq 15\text{-}20\sigma$), and they are discussed further in Appendix B. There are two stars with positive $2\text{-}3\sigma$ excesses (HIP 6485 and HIP 6856), however there are three stars with $2\text{-}3\sigma$ deficits (HIP 9685, GJ 879, and [PZ99] J161318). Hence, the weak excesses for HIP 6485 and HIP 6856 are probably statistical and not real. Excluding the two Upper Sco stars with strong N -band excesses, we find that $56 \pm 12\%$ of the excesses $E(N)$ are within 1σ of zero, and $88 \pm 15\%$ are within 2σ (uncertainties reflect Poisson errors). It does not appear necessary to introduce a non-zero uncertainty in the intrinsic $(K_s - N)_{phot}$. If one wanted to force 68% of the residuals to be within $\pm 1\sigma$ and 95% to be within $\pm 2\sigma$, then either

$\sigma[(K_s - N)_{phot}] \simeq 0.07\text{--}0.09$ mag, or our observational uncertainties are underestimated by $\sim 40\%$. We searched for, and could not find, a plausible reason why our photometric errors would be underestimated by such a large amount. The observations of our standard stars certainly do not support a significant increase in our quoted photometric errors. More calibration observations are required to see if this dispersion can be attributed to actual structure in the intrinsic $(K_s - N)$ colors of normal dwarf stars as a function of spectral type.

Among the Tuc-Hor stars, only one star has as observed N -band flux $\geq 3\sigma$ above that expected for stellar photosphere: HIP 6856 (3.0σ excess). However, there is a Tuc-Hor member with a similarly sized flux *deficit* (HIP 9685; -2.9σ), so it is difficult to claim that the excess for HIP 6856 is statistically significant. *We find that none of the 14 Tuc-Hor members has an N -band excess more than 3σ offset from the dwarf color relation.* We estimate a conservative upper limit to the N -band excess due to a hypothetical dust disk as $3\times$ the uncertainty in the flux excess ($\sigma[E(N)]$; given in column 8 of Table 4).

4. DISK MODELS

Our survey was designed to be sensitive enough to detect the photospheres of young stars, hence we can place meaningful constraints on the census of even optically-thin circumstellar disks in our target sample. We analyze the upper limits to possible mid-IR excess for the Tuc-Hor stars using three different models. The first model assumes a geometrically-thin, optically-thick disk with a large inner hole. The second model assumes emission from an optically-thin disk of single-sized grains. The third model treats the hypothetical disks as a scaled-up version of the zodiacal dust disk in our solar system.

4.1. Optically-Thick Disk With Inner Hole

Infrared and submillimeter observations of T Tauri stars in dark clouds show that roughly half are orbited by an optically-thick circumstellar dust disk (see review by Beckwith 1999). While the stars in our sample are roughly an order of magnitude older (~ 30 Myr) than typical T Tauri stars in dark clouds (≤ 3 Myr), we can ask the question: If the Tuc-Hor stars have optically-thick, geometrically-thin disks, what is the minimum inner hole radius allowed by observations?

To answer this question for each star, we adopt the axisymmetric, geometrically-thin,

optically-thick disk model of Adams, Lada, & Shu (1987), and follow the formalism of Beckwith et al. (1990). While we assume a face-on orientation ($\theta = 0$), our results are not strongly dependent on this assumption. We also assume that the disk is optically-thick between r_{in} and r_{out} (300 AU is assumed for all models) and at all frequencies ($1 - e^{-\tau_\nu} \sim 1$). This is a safe assumption for T Tauri star disks in the wavelength regime probed in this study ($\lambda \leq 100 \mu\text{m}$; Beckwith et al. 1990).

Our N -band photometry alone allows us to rule out optically-thick disks with inner hole radii of ~ 0.1 AU for the Tuc-Hor stars. Stronger constraints on inner disk radius for a hypothetical optically-thick circumstellar disk can be calculated by including IRAS photometry. For IRAS point sources, we adopt $25 \mu\text{m}$, $60 \mu\text{m}$, and $100 \mu\text{m}$ fluxes and upper limits from the Faint Source Catalog (Moshir et al. 1990). Where no IRAS point source is detected, we adopt the IRAS Point Source Catalog upper limits of 0.5 Jy ($25 \mu\text{m}$), 0.6 Jy ($60 \mu\text{m}$), and 1.0 Jy ($100 \mu\text{m}$) (IPAC 1986). For the brightest stars, the IRAS $60 \mu\text{m}$ and $100 \mu\text{m}$ data provide the strongest constraints on the existence of an optically thick disk, whereas for the fainter K and M-type stars, the MIRAC photometry provides the strongest constraint. IRAS did not map the region around HD 105, hence the inner hole radius we derive for this star is based only on the MIRAC N -band 3σ upper limit. In Fig. 2, we illustrate a typical example (HIP 1481) of how the MIRAC and IRAS photometry constrain the existence of optically-thick disks around the Tuc-Hor stars. The values we derive for the minimum inner hole radius for a hypothetical optically-thick disk are given in column 5 of Table 6. The median value of the minimum inner hole radius is ~ 0.3 AU (range: 0.1–7.9 AU). The N -band and IRAS upper limits place the strongest constraints on inner hole size for the luminous F stars ($r_{in} \gtrsim 5$ AU), and the weakest constraints for the faint K/M stars ($r_{in} \gtrsim 0.1$ AU). *The MIRAC and IRAS photometry easily rule out the existence of optically-thick disks with inner hole radii of ~ 0.1 AU of the ~ 30 Myr-old Tuc-Hor stars.*

4.2. Optically-Thin Disk

In the absence of circumstellar gas, a putative mid-IR excess around a ~ 30 -Myr-old star would be most likely to be due to an optically-thin debris disk rather than an optically-thick T Tauri-type disk. The stellar ages ($\sim 10^{7.5}$ yr) are orders of magnitude greater than the Poynting-Robertson drag timescale ($\sim 10^{3-4}$ yr) for typical interplanetary dust grains orbiting ~ 1 AU from a solar-type star. Small dust grains must be continually replenished by collisions of larger bodies, or else they would be only detectable for astrophysically short timescales. Using a simple, single grain-size model, we place upper limits on the amount of

orbiting dust within several AU of the ~ 30 -Myr-old Tuc-Hor stars.

Circumstellar dust grains surrounding young main sequence stars should most likely have radii somewhere between the scale of typical ISM grains (~ 0.01 - $1\ \mu\text{m}$; Mathis, Rumpl, & Nordsieck 1977) and solar system zodiacal dust (~ 10 - $100\ \mu\text{m}$; Grün et al. 1985). Theoretically, an ensemble of dust grains produced from a collisional cascade of fragments is predicted to follow the equilibrium power-law size distribution (Dohnanyi 1969): $n(a) da = n_o a^{-p} da$, where $p = 3.5$. Indeed this power law distribution is observed for ISM grains (Mathis, Rumpl, & Nordsieck 1977) and asteroids (Greenberg & Nolan 1989). With $p = 3.5$, most of the mass is in the largest (rarest) grains, but most of the surface area in the smallest (most common) grains. If the grain size distribution has a minimum cut-off, the mean grain size is calculated to be $\bar{a} = 5a_{min}/3$ (e.g. Metchev, Hillenbrand, & Meyer 2004). A limit on the minimum grain size a_{min} can be estimated from consideration of radiation pressure blow-out (e.g. Artymowicz 1988):

$$a_{min} = \frac{3L_* Q_{pr}}{16\pi G M_* c \rho} \quad (3)$$

Where L_* is the luminosity of the star, Q_{pr} is the radiation pressure efficiency factor averaged over the stellar spectral energy distribution, G is the Newtonian gravitational constant, M_* is the mass of the star, c is the speed of light, and ρ is the grain density (assumed to be 2.5 g cm^{-3} ; Grün et al. 1985). The minimum grain size corresponds to the case where the ratio of the radiation pressure force to the stellar gravitational force is $F_{rad}/F_{grav} = 1$. For this calculation we assume the geometric optics case where $Q_{pr} = 1$. For the idealized grain orbiting the Sun at 1 AU, we calculate $a_{min} = 0.2\ \mu\text{m}$ and $\bar{a} = 0.4\ \mu\text{m}$. The grain size lower limit may be larger if the momentum imparted by stellar winds dominates radiation pressure. The minimum grain size will be somewhat lower if we calculate Q_{pr} using Mie theory and stellar spectral energy distributions, instead of adopting the geometric optics case. Highlighting the uncertainty in this calculation, we note that the value of \bar{a} that we calculate for the Sun is $\sim 10^2 \times$ smaller than the mean interplanetary dust particle orbiting in the Earth’s vicinity (Grün et al. 1985). This is largely due to a complex interplay between Poynting-Robertson drag and collisions. Increasing the cross-section of dust particles in the solar system zodiacal dust cloud by $\sim 10^4$ (i.e. comparable to what we are sensitive to in Tuc-Hor, see §4.3), will decrease the collision timescale, and correspondingly decrease the mean particle size to comparable to the blow-out grain size (Dominik & Decin 2003).

We model the thermal emission from an optically-thin disk of single-sized dust grains of radius \bar{a} orbiting in an annulus between inner radius r_{in} and outer radius r_{out} . Spherical grains emit thermally at a temperature T_d where the incident energy flux from the star

is equal to the isotropically emitted output energy flux of the grain. We approximate the emissivity ϵ_λ of the single-size dust grains by using the simple model of Backman & Paresce (1993): emissivity $\epsilon_\lambda = 1$ for $\lambda < 2\pi a$, and $\epsilon_\lambda = (\lambda/2\pi a)^{-\beta}$ for longer wavelengths, where we assume $\beta = 1.5$. Our adopted value of β is similar to that observed for zodiacal dust (see Fig. 2 of Fixsen & Dwek 2002) and ISM grains (Backman & Paresce 1993). The mass opacity is calculated as $\kappa_\lambda = 3\epsilon_\lambda/4a\rho$. The optical depth of emission through the disk annulus is $\tau_\lambda = \Sigma\kappa_\lambda$, where Σ is the surface density of the disk in g cm^{-2} . We calculate the orbital distance from the star (r) of dust grains heated to temperature T using equation #5 from Wolf & Hillenbrand (2003). We verify that this relation is valid by comparing our calculations with Backman & Paresce (1993) for grains much larger than the Wien peak of incident light (blackbody case) and for grains much smaller than the Wien peak of incident light (e.g. ISM grains). For the Tuc-Hor stars, the Wien peak of incident starlight is comparable to \bar{a} . We assume a flat mass surface density profile ($\Sigma = \Sigma_o r_{AU}^{-p}$; $p = 0$), which is appropriate for a population of dust grains in circular orbits subject to Poynting-Robertson drag (see discussion in §4.1 of Wolf & Hillenbrand 2003, and references therein). This predicted power law is close to what is observed for the zodiacal dust disk in our own solar system ($p = 0.34$; Kelsall et al. 1998).

Where exactly to define the inner and outer radii of a hypothetical dust disk requires some basic modeling. Among the Tuc-Hor stars, 90% of the thermal emission from our hypothetical disk model at N -band comes from within $\approx 1.5\text{-}2.2 \times r_W$ of the star, where r_W is the radius at which the dust is at the Wien temperature (T_W) for the isophotal wavelength of the N -band filter, and $T_W = 2898\lambda_{\mu\text{m}}^{-1}(5/(\beta+5))$ (eqn. 6.9 of Whittet 2003). For simplicity, we adopt a consistent definition of the outer radius for all stars as $2 \times r_W$. Beyond $2 \times r_W$, the hypothetical dust disk contributes negligible flux ($\lesssim 10\%$) to what is observed in the N -band filter. Approximately 50% of the thermal emission observed in N -band from a hypothetical dust disk comes from within $\lesssim 0.4\text{-}0.5 \times r_W$ of the star. For r_{in} , we adopt the radius for which the grain temperature is 1400 K – approximately the silicate dust sublimation limit. The temperatures of the inner edges of typical T Tauri star disks appear to be near this value (Muzerolle et al. 2003). For the Tuc-Hor stars, $r_{in} \sim 0.05$ AU and $r_{out} \sim 10 - 15$ AU. Hence we are most sensitive to dust at orbital radii comparable to our inner solar system.

Results for a typical set of fitted model parameters for our optically-thin disk model are illustrated in Fig. 2. Our calculations suggest that the survey was sensitive to dust disk masses of $\sim 2 \times 10^{-6} M_\oplus$ ($\sim 10^{22}$ g) in a single-sized dust grain population (of uniform size \bar{a} , typically $0.1\text{-}2 \mu\text{m}$). Our optically-thin model puts upper limits of $\Sigma_o \simeq 10^{-6}\text{-}10^{-5} \text{ g cm}^{-2}$ on the surface density of micron-sized dust grains in the $\sim 0.1\text{-}10$ AU region around the Tuc-Hor stars. *For the masses and surface densities quoted, we assume that all of the mass is in dust grains of size \bar{a} .* In order to convey how sensitive our assumptions are for our final results,

we show the effects of changing various parameters on our results in Table 7. The dust disk masses that we calculate are similar to those found by other studies (Chen & Jura 2001; Metchev, Hillenbrand, & Meyer 2004) which also use the single grain-size approximation. The dust mass surface density upper limits that we calculate are $\sim 10^{-7}$ - $10^{-6} \times$ that of the solids in the minimum mass solar nebula (Weidenschilling 1977), however we are not sensitive to bodies much larger than the wavelength of our observations, or to gas.

4.3. Single-Temperature Zody Disk

Another simple model to apply to our data is that of a scaled-up version of the terrestrial-zone zodiacal dust cloud in our own solar system. Though the detailed zodiacal dust model for the inner solar system is quite complex (Kelsall et al. 1998), it can also be approximated by a single temperature blackbody ($T = 260$ K) with bolometric luminosity $8 \times 10^{-8} L_{\odot}$ (Gaidos 1999). This luminosity and temperature imply an equivalent surface area of $5 \times 10^{-6} \text{ AU}^2 \simeq 1 \times 10^{21} \text{ cm}^2$. Gaidos (1999) defines this area as 1 “zody” (1 \mathcal{Z}). The unit is useful for comparing relative amounts of exozodiacal dust between the Sun and other stars.

With none of our stars having statistically significant N -band excesses, we calculate upper limits to the number of zody present using $3 \times$ the uncertainty in the excess measurement, assuming $T_d = 260$ K, and blackbody emission from large grains (i.e. analogous to the situation for the solar system zodiacal dust disk). An upper limit on the fraction of grain thermal emission to stellar emission ($f_d = L_{\text{dust}}/L_*$) was also calculated for each star using these assumptions. While the MIRAC photometry is capable of detecting ~ 4000 \mathcal{Z} disks at $T = 260$ K (equivalent $\log(f_d) < -2.9$) around the Tuc-Hor members observed, no convincing mid-IR excesses were detected.

For completeness, we note that the fraction of disk luminosity to stellar luminosity ($f_d = L_d/L_*$) has been observed to fall off as $f_d \propto age^{-1.76}$ (Spangler et al. 2001). The disk fractional luminosity is predicted to follow $f_d \propto age^{-2}$ if the observed amount of dust is proportional to the collision frequency of large particles, and P-R drag is the dominant dust removal mechanism. Recently, Dominik & Decin (2003) argue that for the very luminous debris disks that have been detected so far, the collision timescales are much shorter than the P-R drag timescales, all the way down to the blow-out grain size. For this collision-dominated scenario, Dominik & Decin (2003) predict that the dust luminosity evolves as $f_d \propto age^{-1}$. While these models ignore effects like, e.g., gravitational perturbations, or ejections, of dust-producing planetesimals by planets (which likely had an enormous effect on the early evolution of the asteroid belt in our solar system), they provide simple, physically plausible models with which to compare observations.

If one takes the solar system zodiacal dust disk ($\log(f_d) \simeq -7.1$, at $\log(\text{age}_{\text{yr}})=9.66$), and scale it backward in time according to Spangler et al’s relation ($f_d \propto \text{age}^{-1.76}$) or the theoretical P-R drag-dominated evolution ($f_d \propto \text{age}^{-2}$), one would predict at age 30 Myr zodiacal dust disks with $\log(f_d) \simeq -3.3$ (6900 \mathcal{Z}) or $\log(f_d) \simeq -2.7$ (23000 \mathcal{Z}), respectively. Hence, for the simple model of collisionally replenished, P-R-drag-depleted disks, *we should have easily detected the solar system’s zodiacal dust disk at age 30 Myr*. For the empirical relation (Spangler et al. 2001), we could have detected the Sun’s zody disk around most (13/15) of the ~ 30 -Myr-old Tuc-Hor stars in our sample. Backward extrapolation of the Sun’s zodiacal dust disk luminosity using Dominik & Decin’s relation for collisionally-dominated disks would yield $\log(f_d) \simeq -4.9$ (150 \mathcal{Z}). Such a disk would not have been detectable in our survey, consistent with our null result. *If* analogs of the Sun’s zodiacal dust disk are common around 30-Myr-old stars, f_d must evolve as a shallower power law (<1.65) than either Spangler et al.’s empirical relation or the P-R-drag-dominated dust depletion model.

5. DISCUSSION

In Fig. 3, we plot the incidence of N -band excess versus stellar age for samples of low-mass stars. While $\sim 80\%$ of ~ 1 -Myr-old stars have in Taurus have N -band excesses (Kenyon & Hartmann 1995), only $\sim 10\%$ of ~ 10 -Myr-old stars in the TW Hya Association and β Pic Moving Group show comparable excess emission (Jayawardhana et al. 1999; Weinberger et al. 2003a,b). Of these ~ 10 -Myr-old stars, only a few are known to have optically-thick disks (TW Hya, Hen 3-600), while the others are optically-thin disks. Our survey imaged a small number ($N=5$) of Upper Sco members (~ 5 -Myr-old) as well, among which two have clear N -band excesses. By an age of ~ 30 Myr, we find that N -band excesses due to optically-thick *or* optically-thin disks, are rare ($\lesssim 7\%$). Excluding the ~ 10 -Myr-old star β Pic, Aumann & Probst (1991) find only one star (ζ Lep) among a sample of 548 field AFGK stars ($\approx 0.2\%$) with a convincing $12\mu\text{m}$ excess. These results seem to imply that *dust appears to be efficiently removed from < 5 -10 AU of young stars on timescales similar to that of the cessation of accretion*. While accretion terminates over a wide range of ages (~ 1 -10 Myr; Haisch, Lada, & Lada 2001a; Hillenbrand et al. 2004), the *duration* of the transition from optically-thick to optically-thin has been observed to be remarkably short ($\sim 10^5$ yr; Skrutskie et al. 1990; Wolk & Walter 1996).

Gravitational perturbations of small planetesimals (~ 0.1 -100 km radius) by growing planetary embryos (~ 2000 km radius) can theoretically cause collisional cascades of dust grains that produce observable mid-IR signatures (Kenyon & Bromley 2004). Simulations show that when the largest planetary embryos reach radii of ~ 3000 km, the population of

dust-producing ~ 0.1 -100 km-size planetesimals in the planet-forming zone becomes collisionally depleted, and N -band excesses become undetectable. The timescale over which the N -band excess would be detectable during this phase of terrestrial planet formation is of order ~ 1 Myr. With a larger sample size (e.g. FEPS Spitzer Legacy survey), one might be able to probe whether this is occurring around stars at age ~ 30 Myr. With 10% of ~ 10 Myr-old stars having detectable N -band excesses (Jayawardhana et al. 1999; Weinberger et al. 2003a,b), we may be witnessing the signature from runaway protoplanet growth in the terrestrial planet zone (Kenyon & Bromley 2004). This would agree with the isotopic evidence in our own solar system that Moon- to Mars-sized protoplanetary embryos accreted within the first ~ 10 -20 Myr (Kleine et al. 2002; Kleine, Mezger, & Münker 2003), ultimately leading to the formation of the Earth-Moon system.

6. CONCLUSIONS

We have undertaken a mid-IR survey of 14 young stars in the nearby ~ 30 -Myr-old Tuc-Hor Association in order to search for emission from warm circumstellar disks. No excess emission at $10\mu\text{m}$ was detected around any Tuc-Hor members. If optically-thick disks do exist around these stars, their inner holes must be large (range: 0.2-5.8 AU). Combining our photometric results with optically-thin dust disk models, we place the following physical constraints on dust orbiting within ~ 10 AU of these ~ 30 -Myr-old stars: fractional disk luminosities of $L_{\text{dust}}/L_* < 10^{-2.9}$ and dust emitting surface areas $< 4000\times$ that of the inner solar system zodiacal dust. The disk masses of micron-size dust grains with orbital radii between the silicate dust sublimation point and ~ 10 AU must be less than $\sim 10^{-6} M_{\oplus}$. The photometric upper limits also suggest that the upper limit on the surface density of micron-sized grains is $\sim 10^{-7} \text{ g cm}^{-2}$. These results imply that inner disks dissipate on timescales comparable to the cessation of accretion.

For their technical support during the MIRAC runs at Magellan, we would like to thank Brian Duffy (Steward Observatory) and the staff of the Las Campanas Observatory: Emilio Cerda, Oscar Dulhalde, Patricio Jones, Gabriel Martin, Mauricio Navarette, Hernan Nuñez, Frank Perez, Hugo Rivera, Felipe Sanchez, Skip Schaller, and Geraldo Valladares. We thank Lissa Miller, Nick Siegler, and Lynne Hillenbrand for critiquing the manuscript. E. E. M. gratefully acknowledges a NASA Graduate Student Fellowship (NGT5-50400) for support. E. E. M. and M. R. M. are supported by the Spitzer Space Telescope Legacy Science Program, provided by NASA through Contract Number 1224768 administered by the Jet Propulsion Laboratory, California Institute of Technology under NASA contract 1407. M.C. thanks NASA for supporting his participation in this work through JPL contract #1224634 with

UC Berkeley. MIRAC is supported through SAO and NSF grant AST 96-18850. BLINC is supported through the NASA Navigator program.

A. Appendix: MIRAC Photometric Calibration

With a significant body of MIRAC-BLINC observations acquired during the 2001-2003 observing runs at Magellan I, it was decided to calculate the photometric attributes of commonly used MIRAC bands on the Cohen-Walker-Witteborn (CWW) system of absolute infrared calibration (e.g. Cohen, Wheaton, & Megeath 2003, and references therein). The photometric standard system for previously published MIRAC studies is given in Appendix 2 of the MIRAC3 User’s Manual (Hoffmann & Hora 1999).

Relative spectral responses (RSRs) for each combination of filter and window were constructed. The throughput chain consists of the following groups of components: atmosphere, telescope optics, BLINC optics, MIRAC optics, and MIRAC detector. The complete throughput equation consists of the following components multiplied together: atmosphere, 3 aluminum mirrors (Magellan), dewar window (KRS-5 or KBr), KBr lens (in BLINC), 5 gold mirrors (3 in BLINC, 2 in MIRAC), filter, and the Si:As array. Most of the MIRAC observations were taken in just four of the seventeen filters currently available in the three MIRAC filter wheels: L , N , 11.6, and Q_s , and these were the filters we absolutely calibrated. For each MIRAC filter, we list a manufacturer’s name, mean filter wavelength (λ_o), bandwidth ($\Delta\lambda/\lambda$; defined as the FWHM of the normalized transmission curve divided by the mean wavelength), and the temperature at which the filter profile was measured (or extrapolated). The transmission profiles for the filters are plotted in Fig. 4. While we list *mean* filter wavelengths (λ_o) in this discussion, the *isophotal* wavelengths (λ_{iso}) are given in Table 8.

The L filter (OCLI “Astro L”; $\lambda_o = 3.84\mu\text{m}$; $\Delta\lambda/\lambda = 16.2\%$; 77 K) is the same one used in all previous and current MIRAC L-band observations, and the transmission curve is plotted in Fig. A2.2 of Hora (1991). The N filter (OCLI code W10773-8; $\lambda_o = 10.75\mu\text{m}$; $\Delta\lambda/\lambda = 47.2\%$; Ambient) was purchased in 1994 in preparation for comet Shoemaker-Levy-9 observations, and has been in use ever since. Pre-1994 MIRAC observations employed a slightly bluer wideband N filter whose characteristics we only present here for completeness (OCLI code W10575-9; $\lambda_o = 10.58\mu\text{m}$; $\Delta\lambda/\lambda = 45.8\%$; Ambient). The narrow 11.6 μm filter (OCLI “Astronomy R”; $\lambda_o = 11.62\mu\text{m}$; $\Delta\lambda/\lambda = 9.5\%$; extrapolated to 5 K) has been used since MIRAC was commissioned (Hora 1991). Its transmission curve includes the effects of a BaF₂ blocker, and it is the only filter of the four that we were able to linearly extrapolate its transmission characteristics to the detector’s operating temperature (5 K; data

at Ambient and 77 K were available). The Q_s or “Q-short” filter has also been used for the lifetime of MIRAC, and its characteristics are only currently known at ambient temperature: $\lambda_o = 17.50 \mu\text{m}$; $\Delta\lambda/\lambda = 10.6\%$).

We followed Cohen et al. (1999) in using PLEXUS (Clark 1996) to assess mean, site-specific atmospheric transmission. Transmission curves for KRS-5 and KBr were taken from the Infrared Handbook (Wolfe & Zissis 1985). We used a KRS-5 window during the August 2001 and May 2002 runs, and a KBr window for the August 2002 and March 2003 runs. The reflectivities of the gold and aluminum mirrors were assumed to be flat in the wavelength range of interest (2-20 μm). The quantum efficiency for the MIRAC doped-silicon blocked-impurity-band (BIB) array was taken from Stapelbroek et al. (1995), following Hoffmann et al. (1998). The zero magnitude attributes of the MIRAC filter systems are given in Table 8. Standard star fluxes on the CWW system for the four primary MIRAC filters (with the KRS-5 dewar window) are given in Table 9. When the KBr dewar window is used on MIRAC-BLINC, the standard star fluxes are nearly identical (to within $<7\%$ of the quoted flux uncertainties), so the same fluxes and magnitudes can be safely adopted. The flux densities in Tables 4 and 5 are referenced to this system.

B. Appendix: Comments on Individual Sources

The only young stars in our survey to show a significant N -band excess were the T Tauri stars HD 143006 and [PZ99] J161411.0-230536, both members of the ~ 5 -Myr-old Upper Sco OB subgroup. Both stars are targets in the FEPS Spitzer Legacy Science program, but only HD 143006 was previously known to possess a circumstellar disk. Both were detected by IRAS, and the MIRAC N -band fluxes are consistent with the color-corrected $12 \mu\text{m}$ measurements in the IRAS FSC (Moshir et al. 1990). Here we discuss these stars in more detail.

B.1. [PZ99] J161411.0-230536

J161411 is a K0-type weak-lined T Tauri ($\text{EW}(\text{H}\alpha) = 0.96 \text{\AA}$) star discovered by Preibisch et al. (1998). In a spectroscopic survey to identify new members of Upper Sco (Mamajek, Meyer, & Liebert, in prep.), the authors obtained a red, low-resolution spectrum of J161411 in July 2000, which shows an asymmetric $\text{H}\alpha$ feature with blueshifted emission and redshifted absorption (net $\text{EW}(\text{H}\alpha) = 0.36 \text{\AA}$). We confirm the strong lithium absorption ($\text{EW}(\text{Li } \lambda 6707) = 0.45 \text{\AA}$) observed by Preibisch et al. (1998). The UCAC2 proper motion (Zacharias et al.

2003) for J161411 is consistent with membership in the Upper Sco subgroup. The $(K_s - N)$ color ($=2.1$) is similar to that of classical T Tauri stars in Taurus-Auriga (Kenyon & Hartmann 1995). The photometric and spectroscopic evidence suggest that this ~ 5 -Myr-old, $\sim 1 M_\odot$ star is actively accreting from a circumstellar disk.

B.2. HD 143006

HD 143006 is a G5Ve (Henize 1976) T Tauri star with strong Li absorption ($\text{EW}(\text{Li } \lambda 6707) = 0.24 \text{ \AA}$; Dunkin, Barlow, & Ryan 1997). The star is situated in the middle of the Upper Sco OB association, and its proper motion ($\mu_\alpha, \mu_\delta = -11, -20 \text{ mas/yr}$; Zacharias et al. 2003) and radial velocity (-0.9 km/s ; Dunkin, Barlow, & Ryan 1997) are indistinguishable from other association members (de Bruijne 1999). Several studies have classified HD 143006 as a distant G-type supergiant or “pre-planetary nebula” (Carballo, Wesselius, & Whittet 1992; Kohoutek 2001), however we believe this is erroneous. If HD 143006 were indeed a supergiant at $d = 3.4 \text{ kpc}$ (Pottasch & Parthasarathy 1988), its tangential velocity would be $\sim 370 \text{ km/s}$ – extraordinarily fast for a population I star. The MIRAC N and 11.6 photometry agrees well with the data points in the SED for HD 143006 plotted in Fig. 2 of Sylvester, Skinner, Barlow, & Mannings (1996). The spectral energy distribution for HD 143006 and its optically-thick disk is well-studied from $0.4\text{--}1300 \mu\text{m}$, so we do not discuss this object further.

REFERENCES

- Adams, F. C., Lada, C. J., & Shu, F. H. 1987, *ApJ*, 312, 788
- Agnor, C. B., Canup, R. M., & Levison, H. F. 1999, *Icarus*, 142, 219
- Artymowicz, P. 1988, *ApJ*, 335, L79
- Aumann, H. H. & Probst, R. G. 1991, *ApJ*, 368, 264
- Backman, D. E. & Paresce, F. 1993, *Protostars and Planets III*, 1253
- Beckwith, S. V. W. 1999, *NATO ASIC Proc. 540: The Origin of Stars and Planetary Systems*, 579
- Beckwith, S. V. W., Sargent, A. I., Chini, R. S., & Guesten, R. 1990, *AJ*, 99, 924

- Beichman, C. A., Neugebauer, G., Habing, H. J., Clegg, P. E., & Chester, T. J. 1988, NASA RP-1190, Vol. 1
- Bessell, M. S. & Brett, J. M. 1988, PASP, 100, 1134
- Briceño, C., Hartmann, L. W., Stauffer, J. R., Gagne, M., Stern, R. A., & Caillault, J. 1997, AJ, 113, 740
- Briggs, R. E. 1962, AJ, 67, 710
- Burns, J. A., Lamy, P. L., & Soter, S. 1979, Icarus, 40, 1
- Carballo, R., Wesselius, P. R., & Whittet, D. C. B. 1992, A&A, 262, 106
- Carpenter, J. M. 2001, AJ, 121, 2851
- Chambers, J. E. 2001, Icarus, 152, 205
- Chen, C. H. & Jura, M. 2001, ApJ, 560, L171
- Chiang, E. I. & Goldreich, P. 1997, ApJ, 490, 368
- Clark, F. O. 1996, PLEXUS Version 2.1a, CD-ROM (Hanscom AFB, MA: Phillips Lab., Dir. Geophys., Air Force Mater. Command).
- Cohen, M., Megeath, S. T., Hammersley, P. L., Martín-Luis, F., & Stauffer, J. 2003, AJ, 125, 2645
- Cohen, M., Schwartz, D. E., Chokshi, A., & Walker, R. G. 1987, AJ, 93, 1199
- Cohen, M., Walker, R. G., Barlow, M. J., & Deacon, J. R. 1992, AJ, 104, 1650
- Cohen, M., Walker, R. G., Carter, B., Hammersley, P., Kidger, M., & Noguchi, K. 1999, AJ, 117, 1864
- Cohen, M., Wheaton, W. A., & Megeath, S. T. 2003, AJ, 126, 10
- Cutispoto, G., Pastori, L., Pasquini, L., de Medeiros, J. R., Tagliaferri, G., & Andersen, J. 2002, A&A, 384, 491
- Cutri, R. M. et al. 2003, 2MASS All-Sky Catalog of Point Sources, VizieR Online Data Catalog, 2246, 0
- de Bruijne, J. H. J. 1999, MNRAS, 306, 381

- Dohnanyi, J. W. 1969, *J. Geophys. Res.*, 74, 2531
- Dominik, C. & Decin, G. 2003, *ApJ*, 598, 626
- ESA 1997, *The Hipparcos and Tycho Catalogues*, VizieR Online Data Catalog, 1239, 0
- Dunkin, S. K., Barlow, M. J., & Ryan, S. G. 1997, *MNRAS*, 290, 165
- Fajardo-Acosta, S. B., Beichman, C. A., & Cutri, R. M. 2000, *ApJ*, 538, L155
- Fixsen, D. J. & Dwek, E. 2002, *ApJ*, 578, 1009
- Gaidos, E. J. 1999, *ApJ*, 510, L131
- Ghez, A. M., Neugebauer, G., & Matthews, K. 1993, *AJ*, 106, 2005
- Golay, M. 1974, *Astrophysics and Space Science Library*, 41
- Greenberg, R. & Nolan, M. C. 1989, *Asteroids II*, 778
- Grün, E., Zook, H. A., Fechtig, H., & Giese, R. H. 1985, *Icarus*, 62, 244
- Habing, H. J. et al. 2001, *A&A*, 365, 545
- Haisch, K. E., Lada, E. A., & Lada, C. J. 2001a, *ApJ*, 553, L153
- Haisch, K. E., Lada, E. A., & Lada, C. J. 2001b, *AJ*, 121, 2065
- Harper, D. A., Loewenstein, R. F., & Davidson, J. A. 1984, *ApJ*, 285, 808
- Hartmann, W. K. & Davis, D. R. 1975, *Icarus*, 24, 504
- Hawley, S. L., Gizis, J. E., & Reid, I. N. 1996, *AJ*, 112, 2799
- Henize, K. G. 1976, *ApJS*, 30, 491
- Hillenbrand, L. A., et al. 2004, in prep
- Hillenbrand, L. A., Strom, S. E., Calvet, N., Merrill, K. M., Gatley, I., Makidon, R. B., Meyer, M. R., & Skrutskie, M. F. 1998, *AJ*, 116, 1816
- Hinz, P. M., Angel, J. R. P., Woolf, N. J., Hoffmann, W. F., & McCarthy, D. W. 2000, *Proc. SPIE*, 4006, 349
- Hoffmann, W. F., Hora, J. L., Fazio, G. G., Deutsch, L. K., & Dayal, A. 1998, *Proc. SPIE*, 3354, 647

- Hoffmann, W. F. & Hora, J. L. 1999, MIRAC3 User’s Manual
- Høg, E. et al. 2000, A&A, 355, L27
- Hora, J. L. 1991, Ph.D. Thesis, The University of Arizona
- IPAC, 1986, IRAS Point Source Catalog
- Jayawardhana, R., Hartmann, L., Fazio, G., Fisher, R. S., Telesco, C. M., & Piña, R. K. 1999, ApJ, 521, L129
- Kelsall, T. et al. 1998, ApJ, 508, 44
- Kenyon, S. J. & Bromley, B. C. 2004, ApJ, 602, L133
- Kenyon, S. J. & Hartmann, L. 1995, ApJS, 101, 117
- Kleine, T., Mezger, K., & Münker, C. 2003, Meteoritics & Planetary Science, vol. 38, Supplement, abstract no.5212, 38, 5212
- Kleine, T., Münker, C., Mezger, K., & Palme, H. 2002, Nature, 418, 952
- Kleinmann, S. G., Cutri, R. M., Young, E. T., Low, F. J., & Gillett, F. C. 1986, IRAS Serendipitous Survey Catalog, Tucson, Univ. of Arizona
- Kohoutek, L. 2001, A&A, 378, 843
- Lagrange, A.-M., Backman, D. E., & Artymowicz, P. 2000, Protostars and Planets IV, 639
- Lawson, W. A., Crause, L. A., Mamajek, E. E., & Feigelson, E. D. 2002, MNRAS, 329, L29
- Lawson, W. A., Lyo, A.-R., & Muzerolle, J., 2004, MNRAS, in press
- Lyo, A.-R., Lawson, W. A., Mamajek, E. E., Feigelson, E. D., Sung, E., & Crause, L. A. 2003, MNRAS, 338, 616
- Mamajek, E. E., Meyer, M. R., & Liebert, J. 2002, AJ, 124, 1670
- Marcy, G. W. & Butler, R. P. 2000, PASP, 112, 137
- Mathioudakis, M. & Doyle, J. G. 1993, A&A, 280, 181
- Mathis, J. S., Rumpl, W., & Nordsieck, K. H. 1977, ApJ, 217, 425
- McCaughrean, M. J. & O’Dell, C. R. 1996, AJ, 111, 1977

- Metchev, S. A., Hillenbrand, L. A., & Meyer, M. R. 2004, *ApJ*, 600, 435
- Meyer, M. R. et al., 2004, *ApJS*, submitted
- Meyer, M. R. et al. 2002, *The Origins of Stars and Planets: The VLT View*. Proceedings of the ESO Workshop held in Garching, Germany, 24-27 April 2001, p. 463.
- Moshir, M. & et al. 1990, *IRAS Faint Source Catalogue*, version 2.0
- Mukai, T. & Yamamoto, T. 1982, *A&A*, 107, 97
- Muzerolle, J., Calvet, N., Briceño, C., Hartmann, L., & Hillenbrand, L. 2000, *ApJ*, 535, L47
- Muzerolle, J., Calvet, N., Hartmann, L., & D'Alessio, P. 2003, *ApJ*, 597, L149
- Nelson, G. J., Robinson, R. D., Slee, O. B., Ashley, M. C. B., Hyland, A. R., Tuohy, I. R., Nikoloff, I., & Vaughan, A. E. 1986, *MNRAS*, 220, 91
- Pottasch, S. R. & Parthasarathy, M. 1988, *A&A*, 192, 182
- Preibisch, T., Guenther, E., Zinnecker, H., Sterzik, M., Frink, S., & Roeser, S. 1998, *A&A*, 333, 619
- Preibisch, T. & Zinnecker, H. 1999, *AJ*, 117, 2381
- Probst, R. G. 1983, *ApJS*, 53, 335
- Randich, S., Pallavicini, R., Meola, G., Stauffer, J. R., & Balachandran, S. C. 2001, *A&A*, 372, 862
- Reach, W. T., Morris, P., Boulanger, F., & Okumura, K. 2003, *Icarus*, 164, 384
- Reid, I. N., Kilkenny, D., & Cruz, K. L. 2002, *AJ*, 123, 2822
- Siess, L., Dufour, E., & Forestini, M. 2000, *A&A*, 358, 593
- Siess, L., Forestini, M., & Dougados, C. 1997, *A&A*, 324, 556
- Silverstone, M. D. 2000, *Ph.D. Thesis*, UCLA
- Skrutskie, M. F., Dutkevitch, D., Strom, S. E., Edwards, S., Strom, K. M., & Shure, M. A. 1990, *AJ*, 99, 1187
- Soderblom, D. R., Jones, B. F., Balachandran, S., Stauffer, J. R., Duncan, D. K., Fedele, S. B., & Hudon, J. D. 1993, *AJ*, 106, 1059

- Song, I., Weinberger, A. J., Becklin, E. E., Zuckerman, B., & Chen, C. 2002, *AJ*, 124, 514
- Song, I., Zuckerman, B., & Bessell, M. S. 2003, *ApJ*, 599, 342
- Spangler, C., Sargent, A. I., Silverstone, M. D., Becklin, E. E., & Zuckerman, B. 2001, *ApJ*, 555, 932
- Stapelbroek, M. G., Seib, D. H., Huffman, J. E., & Florence, R. A. 1995, *Proc. SPIE*, 2475, 41
- Stelzer, B. & Neuhäuser, R. 2001, *A&A*, 372, 117
- Stevenson, D. J. 1987, *Annual Review of Earth and Planetary Sciences*, 15, 271
- Sylvester, R. J., Skinner, C. J., Barlow, M. J., & Mannings, V. 1996, *MNRAS*, 279, 915
- Torres, C. A. O., da Silva, L., Quast, G. R., de la Reza, R., & Jilinski, E. 2000, *AJ*, 120, 1410 (TDQ00)
- Torres, C. A. O., da Quast, G. R., de la Reza, R., da Silva, L., & Melo, C. H. F. 2001, *ASP Conf. Ser.* 244: *Young Stars Near Earth*, 43.
- Torres, C. A. O., Quast, G. R., de La Reza, R., da Silva, L., & Melo, C. H. F. 2003, *ASP Conf. Ser.* 287: *Galactic Star Formation Across the Stellar Mass Spectrum*, 439
- van der Blik, N. S., Manfroid, J., & Bouchet, P. 1996, *A&AS*, 119, 547
- Waters, L. B. F. M., Cote, J., & Aumann, H. H. 1987, *A&A*, 172, 225
- Whittet, D. C. B. 2003, *Dust in the Galactic Environment*, 2nd ed., Bristol: Institute of Physics (IOP) Publishing, Series in Astronomy and Astrophysics
- Weinberger, A. J., Becklin, E. E., Zuckerman, B., & Song, I. 2003, *BAAS*, 202, #34.01
- Weinberger, A. J., Becklin, E. E., Zuckerman, B., & Song, I. 2003, *BAAS*, 203, #13.03
- Weidenschilling, S. J. 1977, *Ap&SS*, 51, 153
- Wetherill, G. W. & Stewart, G. R. 1993, *Icarus*, 106, 190
- Wichmann, R., Schmitt, J. H. M. M., Hubrig, S., 2003, *A&A*, 399, 983
- Wolf, S. & Hillenbrand, L. A. 2003, *ApJ*, 596, 603
- Wolfe, W. L. & Zissis, G. J. 1985, Arlington: Office of Naval Research, Department of the Navy

- Wolk, S. J. & Walter, F. M. 1996, *AJ*, 111, 2066
- Wood, B. E., Müller, H., Zank, G. P., & Linsky, J. L. 2002, *ApJ*, 574, 412
- Zacharias, N., Urban, S. E., Zacharias, M. I., Wycoff, G. L., Hall, D. M., Germain, M. E., Holdenried, E. R., & Winter, L. 2003, *VizieR Online Data Catalog*, 1289, 0
- Zuckerman, B., Song, I. 2004, *ApJ*, 603, 738
- Zuckerman, B., Song, I., Bessell, M. S., & Webb, R. A. 2001, *ApJ*, 562, L87
- Zuckerman, B., Song, I., & Webb, R. A., 2001, *ApJ*, 559, 388 (ZSW01)
- Zuckerman, B. & Webb, R. A., 2000, *ApJ*, 535, 959 (ZW00)

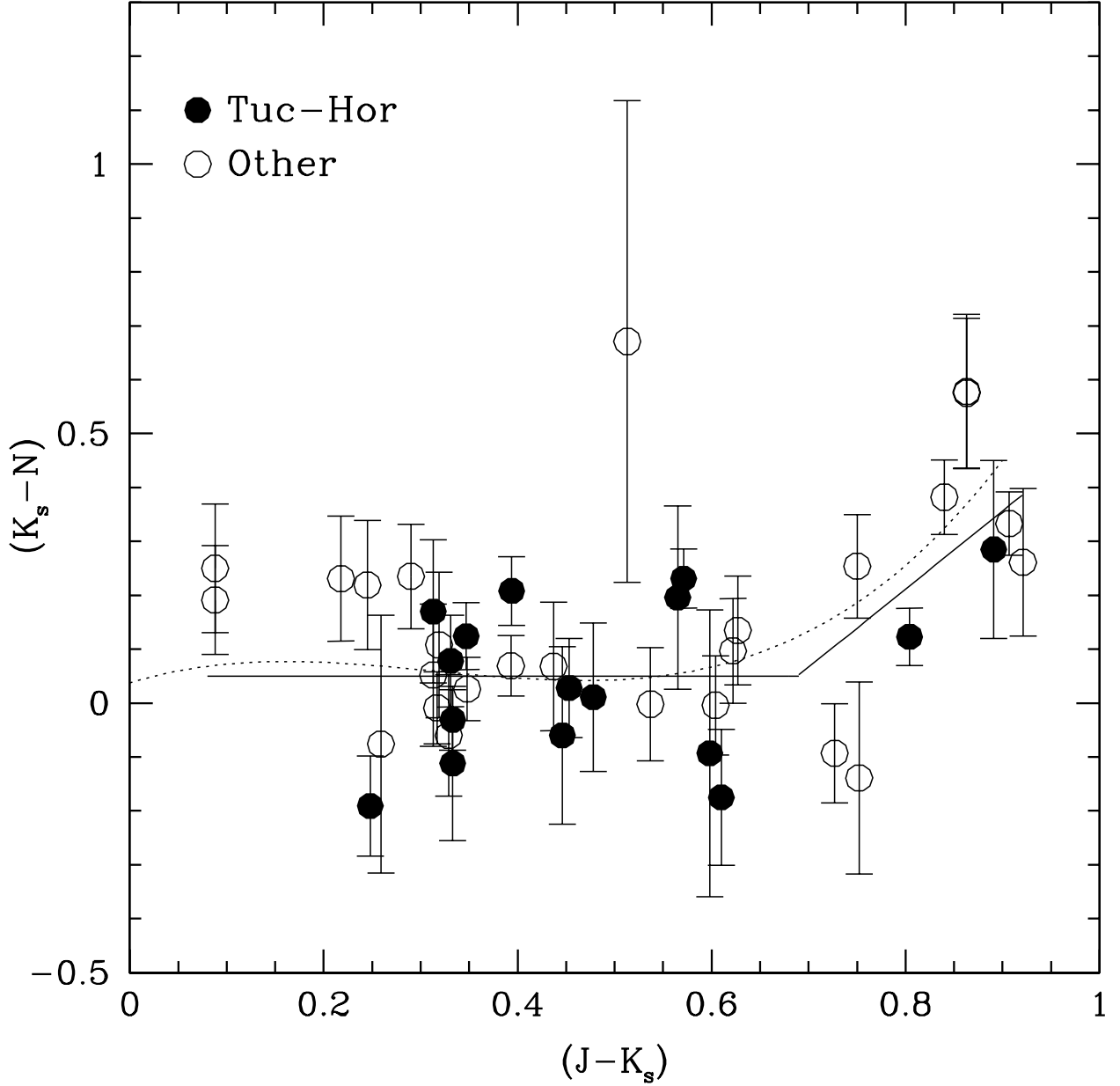


Fig. 1.— Color-color diagram for Tuc-Hor members (*filled circles*) and other stars observed in this study (*open circles*). Two stars (not members of Tuc-Hor) with significantly red ($K_s - N$) colors are not shown (HD 143006 and J161411). The *solid line* is our adopted photosphere color relation (§3). The *dashed line* is a smoothed fit to the $(K_{CIT} - [12])$ dwarf sequence of Kenyon & Hartmann (1995), where we calculate $(K_s - N) \simeq (K_{CIT} - [12])_{KH95} - 0.06$.

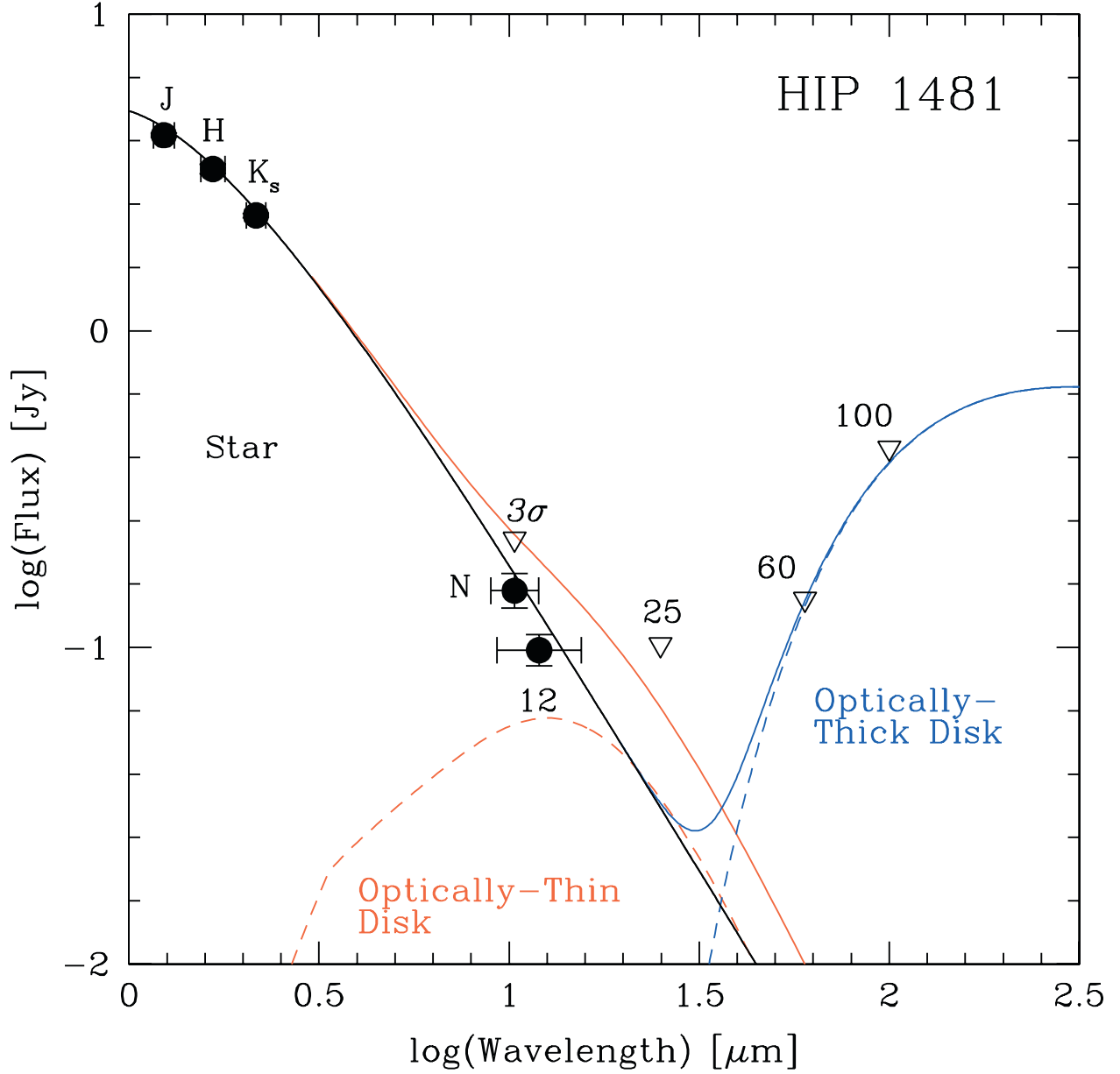


Fig. 2.— Optically-thin and thick dust models fit to the MIRAC and IRAS photometry for a typical Tuc-Hor star (HIP 1481). If the star has an optically-thick disk, its inner hole radius must be >1.8 AU (constrained by IRAS PSC $60\mu\text{m}$ upper limits). The stellar SED is approximated here as a 6026 K blackbody. The optically-thin disk model is conservatively matched to the $3\times$ the uncertainty in the N -band excess $E(N)$. The kink in the spectral energy distribution for the optically-thin model occurs at $\lambda = 2\pi\bar{a}$ due to our simple treatment of dust emissivity (§4.2).

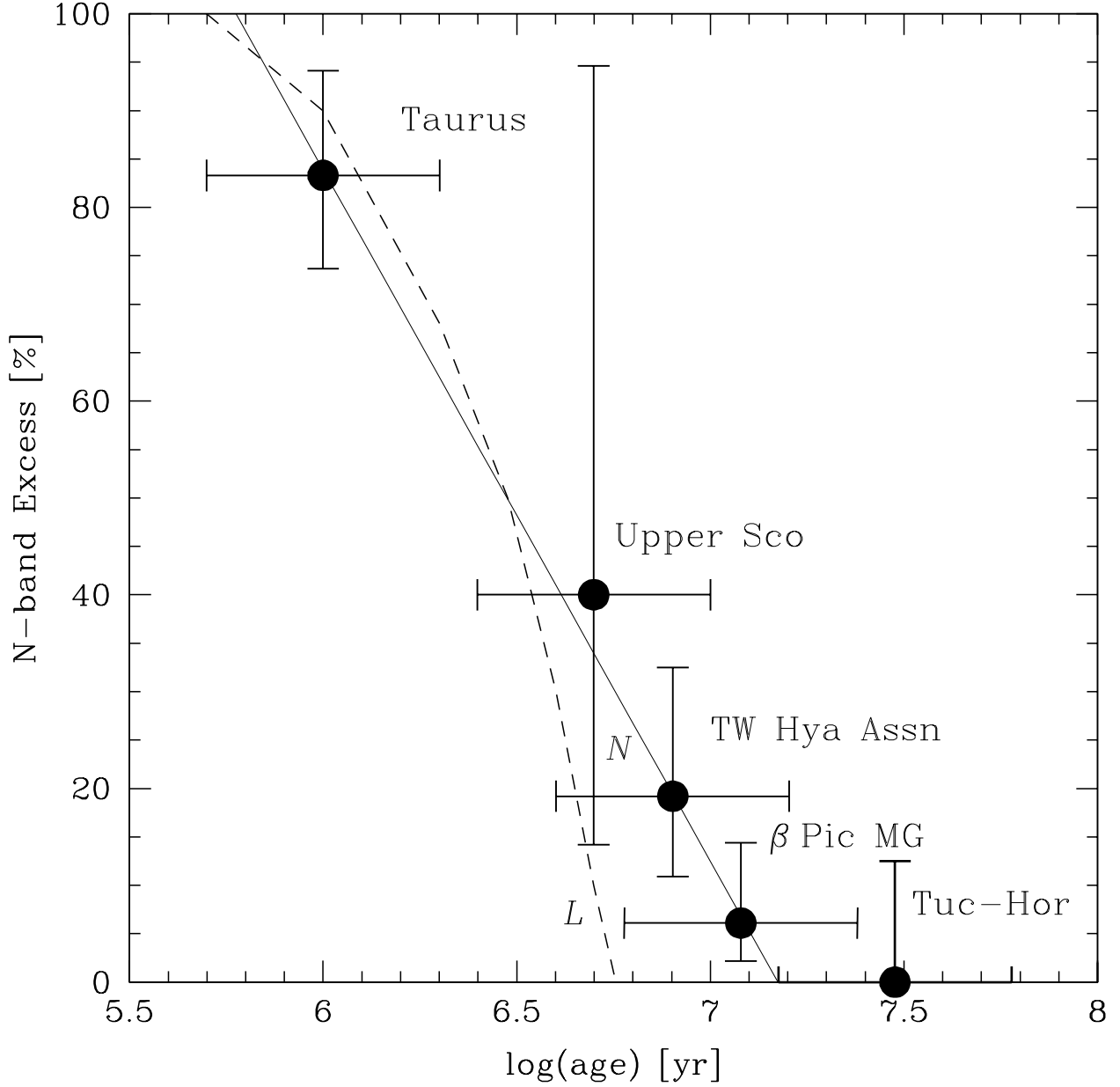


Fig. 3.— N -band excess versus age for stellar samples of varying ages. Data are plotted for the following samples: Taurus-Auriga (Kenyon & Hartmann 1995), TW Hya Association (Jayawardhana et al. 1999; Weinberger et al. 2003a), β Pic group (Weinberger et al. 2003b), Upper Sco, and Tuc-Hor (both this study). Data from the IRAS study of AFGK-type field stars by Aumann & Probst (1991) shows that N -band excesses among mostly older ($\gtrsim 100$ Myr) field stars are extraordinarily rare ($\sim 0.2\%$). *Dashed line* is the L -band disk fraction measured by Haisch, Lada, & Lada (2001a). The *solid line* is a fit to the N -band disk fraction for the four youngest groups. It appears that N -band excesses are only detectable for timescales marginally longer than that of L -band excesses, however the statistics are still poor. Note that in the TW Hya Association, there exists a mix of optically-thick and thin disks, while in the β Pic group, all of the known disks are optically-thin.

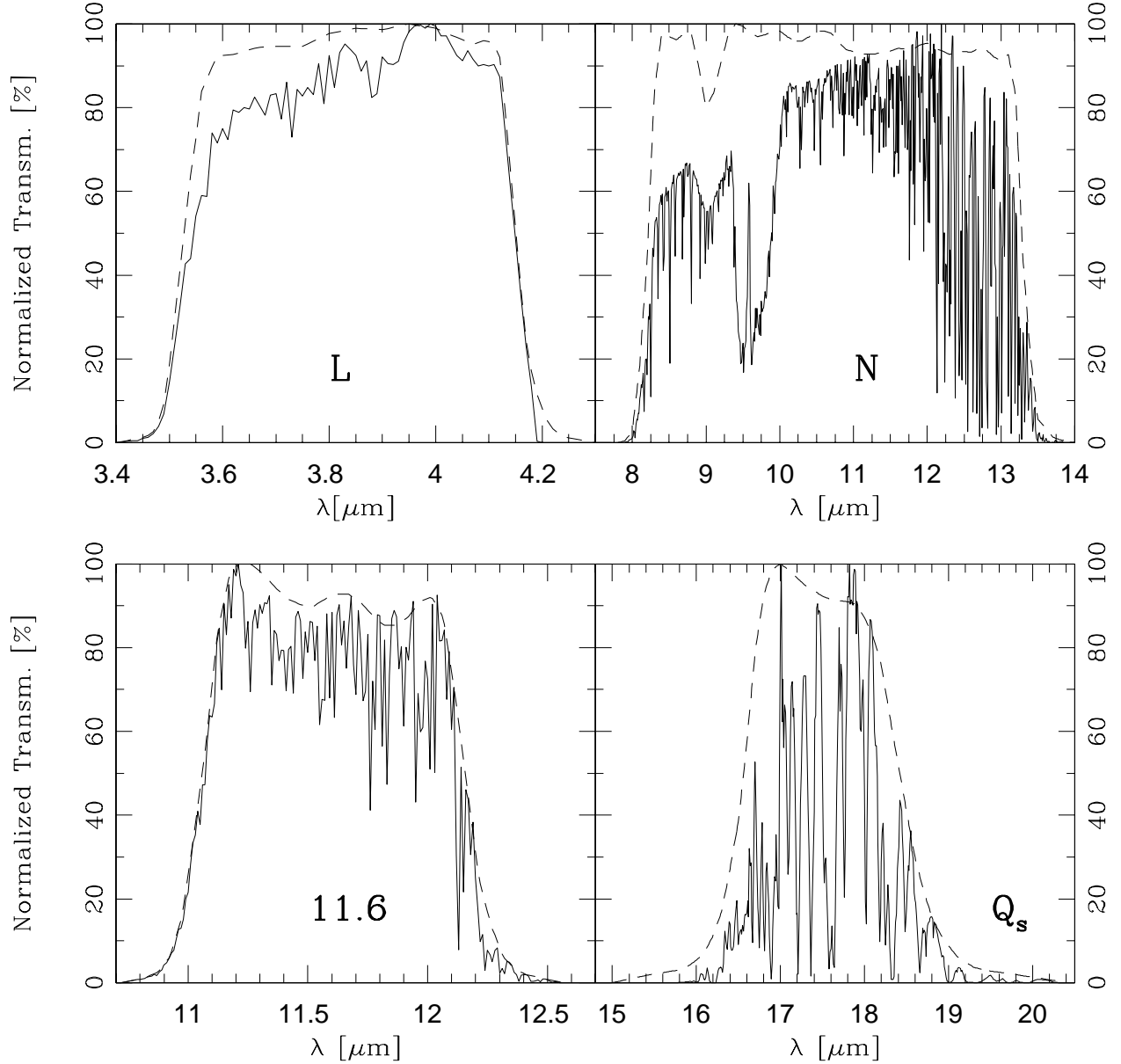


Fig. 4.— Transmission profiles for the MIRAC L , N , 11.6, and Q_s filters. *Dashed lines* are the normalized filter transmission profiles. *Solid lines* are the relative spectral response curves (= “RSRs”, details given in Appendix A), and represent the product of transmissions for the filters, detector, optics, KRS-5 dewar window, and atmosphere. The RSRs were used for absolutely calibrating MIRAC on the CWW system.

Table 1. Age Estimates for Tucana-Horologium Association

(1) Reference	(2) Group	(3) Age (Myr)	(4) Method	(5) Notes
...
Zuckerman & Webb (2000)	Tuc	40	H α Emission	Comparing H α emission of 3 stars to α Per members
Torres et al. (2000)	Hor	30	Theoretical Isochrones	Siess, Forestini, & Dougados (1997) tracks
Torres et al. (2001)	Tuc-Hor	20	Velocity Dispersion	“GAYA” = Tuc-Hor
Stelzer & Neuhäuser (2001)	Tuc	10-30	X-ray Emission	Member L_X values similar to TWA, Tau-Aur, & IC 2602
Zuckerman, Song, & Webb (2001)	Tuc	10-40	Theoretical Isochrones	K & M stars; Siess, Dufour, & Forestini (2000) tracks

Table 2. MIRAC Observations of Tuc-Hor Members

(1)	(2)	(3)	(4)	(5)
UT	Star	Band	On-Source	Flux
Date	Name	...	Time (s)	Standards
2001 Aug 8	HIP 105388	<i>N</i>	300	ι Cet, α CMa
...	HIP 105404	<i>N</i>	600	ι Cet, α CMa
...	HIP 107947	<i>N</i>	600	ι Cet, α CMa
...	HIP 108195	<i>N</i>	360	ι Cet, α CMa
...	HIP 116748AB	<i>N</i>	600	ι Cet, α CMa
...	HIP 1481	<i>N</i>	480	ι Cet, α CMa
...	HIP 1910	<i>N</i>	840	ι Cet, α CMa
...	HIP 2729	<i>N</i>	840	ι Cet, α CMa
2001 Aug 9	HIP 490	<i>N</i>	420	ι Cet, η Sgr, α CMa
...	HIP 6485	<i>N</i>	600	ι Cet, η Sgr, α CMa
...	HIP 6856	<i>N</i>	660	ι Cet, η Sgr, α CMa
...	HIP 9892	<i>N</i>	840	ι Cet, η Sgr, α CMa
...	ERX 37N	<i>N</i>	1020	ι Cet, η Sgr, α CMa
2001 Aug 10	HIP 9685	<i>N</i>	690	α Cen, ι Cet, η Sgr
2002 Aug 21	HIP 1910	<i>N</i>	180	γ Cru, η Sgr, ι Cet

Table 3. MIRAC Observations of Other Stars

(1) UT Date	(2) Star Name	(3) Band ...	(4) On-Source Time (s)	(5) Flux Standards
2001 Aug 6	GJ 799 AB	11.6	135	ι Cet
...	GJ 803	11.6	165	ι Cet
...	HIP 108195	11.6	60	ι Cet
2001 Aug 7	HIP 99273	11.6	255	α Car, α PsA, γ Cru
2001 Aug 8	HD 143006	N	60	ι Cet, α CMa
...	HD 143006	11.6	120	γ Cru
...	[PZ99] J161318.6-221248	N	600	ι Cet, α CMa
...	HD 181327	N	240	ι Cet, α CMa
...	HR 7329	N	60	ι Cet, α CMa
2001 Aug 9	RX J1853.1-3609	N	960	ι Cet, η Sgr, α CMa
...	RX J1917.4-3756	N	660	ι Cet, η Sgr, α CMa
2001 Aug 10	HIP 63797	N	300	α Cen, ι Cet, η Sgr
...	[PZ99] J161411.0-230536	N	360	α Cen, ι Cet, η Sgr
...	ScoPMS 214	N	450	α Cen, ι Cet, η Sgr
...	ScoPMS 5	N	450	α Cen, ι Cet, η Sgr
...	HIP 95149	N	360	α Cen, ι Cet, η Sgr
...	HIP 113579	N	510	α Cen, ι Cet, η Sgr
...	HIP 1134	N	480	α Cen, ι Cet, η Sgr
2002 Aug 21	HIP 93815	N	180	γ Cru, η Sgr, ι Cet
...	HIP 99803 A	N	690	γ Cru, η Sgr, ι Cet
...	HIP 99803 B	N	165	γ Cru, η Sgr, ι Cet
...	HIP 105441	N	360	γ Cru, η Sgr, ι Cet
...	HIP 107649	N	240	γ Cru, η Sgr, ι Cet
...	PPM 366328	N	180	γ Cru, η Sgr, ι Cet
...	HIP 108809	N	360	γ Cru, η Sgr, ι Cet
...	HIP 108422	N	300	γ Cru, η Sgr, ι Cet
...	GJ 879	N	240	γ Cru, η Sgr, ι Cet

Table 4. *N*-band Photometry of Tuc-Hor Members

(1)	(2)	(3)	(4)	(5)	(6)	(7)	(8)
Name	Name	Spec.	K_s	Pred. F_ν	Meas. F_ν	$E(N)$	Dev.
...	...	Type	(mag)	(mJy)	(mJy)	(mJy)	(σ)
HIP 490	HD 105	G0	6.12 ± 0.02	139	138 ± 8	-1 ± 8	-0.2
HIP 1481	HD 1466	F8	6.15 ± 0.02	135	151 ± 20	$+16 \pm 20$	+0.8
HIP 1910	BPM 1699	M0	7.49 ± 0.02	51	49 ± 7	-2 ± 7	-0.3
HIP 2729	HD 3221	K4	6.53 ± 0.02	111	102 ± 5	-9 ± 5	-1.7
HIP 6485	HD 8558	G6	6.85 ± 0.03	71	82 ± 4	$+11 \pm 4$	+2.4
HIP 6856	HD 9054	K2	6.83 ± 0.02	72	85 ± 4	$+13 \pm 4$	+3.0
HIP 9685	HD 12894	F4	5.45 ± 0.02	258	207 ± 17	-51 ± 18	-2.9
HIP 9892	HD 13183	G5	6.89 ± 0.02	68	67 ± 6	-1 ± 6	-0.2
ERX 37N	AF Hor	M3	7.64 ± 0.03	42	46 ± 3	$+4 \pm 3$	+1.3
HIP 105388	HD 202917	G5	6.91 ± 0.02	67	65 ± 9	-2 ± 9	-0.3
HIP 105404	HD 202947	K0	6.57 ± 0.02	92	74 ± 9	-18 ± 9	-1.9
HIP 107947	HD 207575	F6	6.03 ± 0.02	151	155 ± 12	$+4 \pm 12$	+0.3
HIP 108195	HD 207964	F3	4.91 ± 0.02	424	394 ± 20^a	-30 ± 21	-1.4
HIP 116748A	HD 222259A	G6	6.68 ± 0.03	83	75 ± 12	-8 ± 12	-0.7
HIP 116748B	HD 222259B	K	7.03 ± 0.06	60	53 ± 14	-7 ± 14	-0.5

Note. — Columns (1) Hipparcos name, (2) other name, (3) spectral type, from either ZW00, TDQ00, or ZSW01, (4) K_s magnitude from 2MASS (Cutri et al. 2003), (5) measured MIRAC *N*-band flux, (6) predicted photospheric flux, (7) flux excess and uncertainty, (8) residual deviation = $E(N)/\sigma(E(N))$. ERX 37N is given in SIMBAD as [TDQ2000] ERX 37N. Predicted *N*-band photospheric fluxes use or assume: 2MASS K_s magnitudes, $A_V = 0$, dwarf color relations from §3, and zero magnitude flux of 37.25 Jy for *N*-band.

^aHIP 108195 was also imaged at $11.6\mu\text{m}$ with a flux of 284 ± 40 mJy.

Table 5. Measured Photometry for Other Stars

(1) Name ...	(2) Name ...	(3) Spec. Type	(4) K_s (mag)	(5) Band ...	(6) Pred. F_ν (mJy)	(7) Meas. F_ν (mJy)	(8) E(N) (mJy)	(9) Dev. (σ)
Tuc-Hor Rejects								
HD 177171	HIP 93815	F7	3.81 ± 0.10^a	N	1171	1236 ± 103	$+65 \pm 149$	+0.4
HD 191869 A ^b	HIP 99803 A	F7	6.81 ± 0.02	N	74	87 ± 9	$+13 \pm 9$	+1.5
HD 191869 B ^b	HIP 99803 B	...	6.86 ± 0.03	N	70	63 ± 14	-7 ± 14	-0.5
HD 202746	HIP 105441	K2	6.40 ± 0.02	N	107	116 ± 11	$+9 \pm 11$	+0.8
HD 207129	HIP 107649	G0	4.12 ± 0.02^c	N	880	837 ± 70	-43 ± 72	-0.6
PPM 366328	TYC 9129-1361-1	K0	7.61 ± 0.02	N	35	63 ± 24	$+28 \pm 24$	+1.1
HD 208233 ^d	HIP 108422	G8	6.75 ± 0.02	N	78	89 ± 14	$+11 \pm 14$	+0.8
Upper Sco Members + FEPS								
[PZ99] J161411.0-230536	TYC 6793-819-1	K0	7.46 ± 0.03	N	48	273 ± 11	$+225 \pm 11$	+20.3
ScoPMS 214	NTTS 162649-2145	K0	7.76 ± 0.02	N	42	37 ± 5	-5 ± 5	-1.0
ScoPMS 5	HD 142361	G3	7.03 ± 0.02^e	N	60	58 ± 6	-2 ± 6	-0.4
HD 143006	HBC 608	G6/8	7.05 ± 0.03	N	134	648 ± 31	$+514 \pm 31$	+16.5
HD 143006	HBC 608	G6/8	7.05 ± 0.03	11.6	104	640 ± 34	$+536 \pm 34$	+15.7
[PZ99] J161318.6-221248	TYC 6213-306-1	G9	7.43 ± 0.02	N	45	32 ± 6	-13 ± 6	-2.2
β Pic Group Members								
GJ 799 A	HIP 102141 A	M4.5	5.70 ± 0.10^f	11.6	202	259 ± 24	$+57 \pm 30$	+1.9
GJ 799 B	HIP 102141 B	M4	5.70 ± 0.10^f	11.6	202	260 ± 25	$+58 \pm 31$	+1.9
GJ 803	HIP 102409	M0	4.53 ± 0.02	11.6	627	608 ± 32	-19 ± 34	-0.6
HD 181327	HIP 95270	F5/6	5.91 ± 0.03	N	169	200 ± 18	$+31 \pm 19$	+1.7
HR 7329	HIP 95261	A0	5.01 ± 0.03	11.6	301	343 ± 31	$+42 \pm 32$	+1.3
HR 7329	HIP 95261	A0	5.01 ± 0.03	N	387	466 ± 52	$+79 \pm 53$	+1.5
CrA Off-Cloud Stars + FEPS								
RX J1853.1-3609	HD 174656	G6	7.28 ± 0.02	N	48	46 ± 4	-2 ± 4	-0.4
RX J1917.4-3756	SAO 211129	K2	7.47 ± 0.03	N	44	45 ± 4	$+1 \pm 4$	+0.3
Sco-Cen Reject								
HD 113376 ^g	HIP 63797	G3	6.70 ± 0.02	N	81	83 ± 9	$+2 \pm 9$	+0.2
Other FEPS Targets								
HD 181321	HIP 95149	G5	4.93 ± 0.02	N	418	425 ± 21	$+7 \pm 22$	+0.3
HD 191089	HIP 99273	F5	6.08 ± 0.03	11.6	113	132 ± 15	$+19 \pm 15$	+1.3

Table 5—Continued

(1)	(2)	(3)	(4)	(5)	(6)	(7)	(8)	(9)
Name	Name	Spec.	K_s	Band	Pred. F_ν	Meas. F_ν	E(N)	Dev.
...	...	Type	(mag)	...	(mJy)	(mJy)	(mJy)	(σ)
HD 209253	HIP 108809	F6/7	5.39 ± 0.02	N	273	255 ± 21	-18 ± 22	-0.8
HD 216803	GJ 879	K4	3.81 ± 0.02^c	N	1233	1027 ± 85	-206 ± 88	-2.3
HD 217343	HIP 113579	G3	5.94 ± 0.03	N	164	160 ± 8	-4 ± 9	-0.4
HD 984	HIP 1134	F5	6.07 ± 0.02	N	145	131 ± 14	-14 ± 14	-1.0

Note. — (1) Hipparcos name, (2) other name, (3) spectral type (from SIMBAD unless otherwise noted) (4) K_s magnitude from 2MASS (Cutri et al. 2003), unless otherwise noted, (5) measured MIRAC N -band flux, (6) predicted photospheric flux, (7) flux excess and uncertainty, (8) residual deviation = $E(N)/\sigma(E(N))$.

^aStar is saturated in 2MASS. We adopt the V magnitude from Hipparcos (ESA 1997), and the intrinsic $(V - J)$ and $(J - K_s)$ color for F7 stars from Kenyon & Hartmann (1995) (converted to 2MASS system via Carpenter 2001), to calculate a rough K_s magnitude. We assume an uncertainty of 0.10 mag.

^bZuckerman et al. (2001) calls the pair HIP 99803 NE and SW. A = SE and B = NW.

^c2MASS photometry is saturated. We take the K_{CIT} magnitude from Aumann & Probst (1991) and transform it to the 2MASS system via equation (12) of Carpenter (2001).

^dWe can not rule out HIP 108422 as a Tuc-Hor member based on its proper motion, or the agreement between the calculated cluster parallax and Hipparcos trigonometric parallax. However, we conservatively exclude the star as a member at present, since no spectroscopic evidence of youth has been presented in the literature. If it is co-moving with the Tucana nucleus, we predict a RV of $+3 \text{ km s}^{-1}$.

^eA 0.8" binary discovered by Ghez, Neugebauer, & Matthews (1993) and seen in MIRAC K -band images. MIRAC N and 2MASS K_s magnitudes are for unresolved pair.

^fThe 2MASS K_s magnitudes from Reid, Kilkenny, & Cruz (2002) appear to be at odds with the combined magnitude for A & B measured by Cutri et al. (2003), Nelson et al. (1986), and Probst (1983). The system is essentially an equal brightness binary at optical bands as well as at N , so we split the 2MASS K_s magnitude evenly and adopt a generous 0.10 mag error. Spectral types are from Hawley, Gizis, & Reid (1996)

^gRejected as a Sco-Cen member by Mamajek, Meyer, & Liebert (2002)

Table 6. Model Parameters for Tuc-Hor Members

(1)	(2)	(3)	(4)	(5)	(6)	(7)	(8)	(9)	(10)	(11)
Name	π	\log	\log	r_{hole}	\bar{a}	$r_{in} - r_{out}$	Σ_o	M_{disk}	\log	Zodys
...	(mas)	T_{eff}	L/L_\odot	(AU)	(μm)	(AU)	(g cm^{-2})	(M_\oplus)	(L_d/L_*)	(\mathcal{Z})
HIP 490	24.9	3.776	+0.17	0.3	0.50	0.05-13.9	3.4E-06	7.8E-05	-3.25	2.6E3
HIP 1481	24.4	3.780	+0.21	1.8	0.53	0.06-13.8	8.2E-06	1.9E-04	-2.89	6.4E3
HIP 1910	21.6	3.585	-0.81	0.1	0.10	0.03-10.8	1.4E-05	1.9E-04	-2.20	2.9E3
HIP 2729	21.8	3.643	-0.32	0.7	0.27	0.04-12.4	5.0E-06	9.2E-05	-2.80	2.1E3
HIP 6485	20.3	3.744	-0.04	0.3	0.34	0.05-14.4	3.2E-06	7.7E-05	-3.10	2.0E3
HIP 6856	26.9	3.707	-0.55	0.1	0.12	0.04-15.3	2.6E-06	7.1E-05	-2.85	1.1E3
HIP 9685	21.2	3.829	+0.71	4.9	1.44	0.09-12.0	6.9E-06	1.2E-04	-3.45	7.5E3
HIP 9892	19.9	3.752	-0.08	0.2	0.31	0.05-14.9	4.5E-06	1.2E-04	-2.91	3.0E3
ERX 37N	22.6	3.540	-0.89	0.1	0.14	0.02-8.6	8.3E-06	7.1E-05	-2.48	1.2E3
HIP 105388	21.8	3.746	-0.16	0.2	0.26	0.05-15.3	5.4E-06	1.5E-04	-2.75	3.6E3
HIP 105404	21.7	3.719	-0.21	0.2	0.26	0.04-14.6	6.4E-06	1.6E-04	-2.68	3.8E3
HIP 107947	22.2	3.795	+0.38	2.1	0.75	0.06-13.0	6.3E-06	1.3E-04	-3.16	4.8E3
HIP 108195	21.5	3.817	+0.91	7.9	2.40	0.11-11.7	1.0E-05	1.6E-04	-3.53	8.6E3
HIP 116748A	21.6	3.746	-0.09	1.0	0.31	0.05-14.8	8.0E-06	2.1E-04	-2.65	5.0E3
HIP 116748B	21.6	3.645	-0.46	0.2	0.19	0.04-13.0	1.4E-05	2.9E-04	-2.24	5.8E3

Note. — (1) Star name. (2) Parallax. ERX 37N parallax calculated via cluster parallax method, the other values are from Hipparcos (ESA 1997). (3) Stellar effective temperature. (4) Luminosity in solar units. (5) Lower limits on inner hole radius for a hypothetical optically-thick disk (§4.1). (6) Mean calculated grain size, where $\bar{a} = 5a_{min}/3$, where a_{min} is the blow-out grain size (Eqn. 1; §4.2). (7) Inner and outer radii for calculation of optically-thin disk (§4.2). (8) Disk surface mass density for optically-thin disk model (§4.2); independent of radius for our adopted model with ($\Sigma = \Sigma_o r_{AU}^{-p}$; $p = 0$). (9) Upper limit on disk mass (in grains of size \bar{a}) for optically-thin model (§4.2). (10) Upper limit to fractional luminosity of scaled-up zodiacal dust model (§4.3). (11) Upper limit to emitting area of scaled-up zodiacal dust model (in units of “zodys”, where $1 \mathcal{Z} = 10^{21} \text{ cm}^2$; §4.3).

Table 7. Effects of Changing Adopted Values on Model Output

(1) Parameter	(2) Δr_{in}	(3) Δr_{out}	(4) $\Delta \Sigma_o$	(5) ΔM_{dust}	(6) Notes
$\beta = 2$	$\times(1.00-1.17)$	$\times(1.4-2.3)$	$/ (1.3-0.26)$	$\times(1.5-21)$	crystalline case
$\beta = 1$	$/ (1.00-1.16)$	$/ (1.4-2.3)$	$\times(1.2-0.24)$	$/ (1.6-22)$	amorphous case
$\beta = 0$	$/ (1.01-1.74)$	$/ (2.7-12)$	$\times(1.5-0.013)$	$/ (4.7-10700)$	blackbody case
$\bar{a} \times 10$	$/ (1.01-1.73)$	$/ (1.6-4.4)$	$\times(9.5-0.32)$	$\times(3.8-0.017)$...
$\bar{a} \times 100$	$/ (1.01-1.75)$	$/ (1.6-7.1)$	$\times(95-2.7)$	$\times(38-0.054)$...
$p = 0.34$	no change	no change	$\times(1.3-0.6)$	$/ (1.5-2.8)$	zodiacal case
$p = 1$	no change	no change	$\times(1.3-0.17)$	$/ (4.7-26)$...
$p = 1.5$	no change	no change	$/ (1.1-21)$	$/ (13-140)$	min. mass solar nebula case

Note. — Columns: (1) model parameter, (2-5) range of factors acted upon model values in Table 6 if parameter in column #1 is adopted, (6) case name.

Table 8. Zero-Magnitude Attributes of MIRAC Photometric Bands

(1)	(2)	(3)	(4)	(5)	(6)	(7)	(8)
MIRAC	λ_{iso}	Bandwidth	In-Band	$F_{\lambda}(\text{iso})$	Bandwidth	$F_{\nu}(\text{iso})$	$\nu(\text{iso})$
Band	(μm)	(μm)	(W cm^{-2})	($\text{W cm}^{-2} \mu\text{m}^{-1}$)	(Hz)	(Jy)	(Hz)
<i>L</i>	3.844	0.5423	2.631E-15	4.852E-15	1.102E+13	238.8	7.793E+13
uncert.	0.018	0.0037	1.609%	8.469E-17	6.820E+10	4.1	7.361E+11
<i>N</i>	10.35	3.228	3.263E-16	1.011E-16	8.760E+12	37.25	2.946E+13
uncert.	0.05	0.022	1.632%	1.789E-18	4.170E+10	0.60	2.416E+11
11.6	11.57	0.8953	5.816E-17	6.496E-17	2.006E+12	29.00	2.592E+13
uncert.	0.08	0.0135	2.110%	1.686E-18	2.149E+10	0.61	2.827E+11
<i>Q_s</i>	17.58	0.9130	1.123E-17	1.230E-17	8.834E+11	12.72	1.706E+13
uncert.	0.14	0.0185	2.494%	3.951E-19	1.263E+10	0.32	2.171E+11

Note. — Columns (1) name of MIRAC band, (2) isophotal wavelength, (3) wavelength bandwidth of RSR, (4) In-band flux for zero-magnitude star, (5) isophotal monochromatic intensity (wavelength units), (6) frequency bandwidth of RSR, (7) isophotal monochromatic intensity (frequency units), (8) isophotal frequency. Note that the stated quantities assume that a KRS-5 dewar window is used. If the KBr dewar window is used, the values are nearly identical. For KBr, every stated value is within 5% of the stated uncertainty for the *L*, 11.6, and *Q_s* bands, and within 36% of the stated uncertainty for *N*-band.

Table 9. Predicted MIRAC Standard Star Fluxes on CWW system

(1)	(2)	(3)	(4)	(5)	(6)	(7)	(8)	(9)	(10)
HD	Alt.	Band	Mag	unc.	F_λ	unc.	F_ν	unc.	unc.
Name	Name	($\text{W cm}^{-2} \mu\text{m}^{-1}$)	($\text{W cm}^{-2} \mu\text{m}^{-1}$)	(mJy)	(mJy)	(%)
1522	ι Cet	L	0.800	0.022	2.32E-15	4.99E-17	1.14E+05	2.46E+03	2.15
1522	ι Cet	N	0.807	0.021	4.81E-17	9.98E-19	1.77E+04	3.68E+02	2.08
1522	ι Cet	11.6	0.772	0.026	3.19E-17	9.01E-19	1.42E+04	4.02E+02	2.83
1522	ι Cet	Q_s	0.775	0.030	6.02E-18	2.08E-19	6.23E+03	2.16E+02	3.46
12929	α Ari	L	-0.762	0.021	9.79E-15	2.01E-16	4.82E+05	9.88E+03	2.05
12929	α Ari	N	-0.754	0.020	2.02E-16	4.00E-18	7.46E+04	1.47E+03	1.98
12929	α Ari	11.6	-0.789	0.025	1.34E-16	3.70E-18	6.00E+04	1.65E+03	2.75
12929	α Ari	Q_s	-0.787	0.030	2.54E-17	8.63E-19	2.62E+04	8.93E+02	3.40
29139	α Tau	L	-3.045	0.021	8.01E-14	1.62E-15	3.94E+06	7.99E+04	2.03
29139	α Tau	N	-3.013	0.020	1.62E-15	3.21E-17	5.97E+05	1.18E+04	1.98
29139	α Tau	11.6	-3.074	0.025	1.10E-15	3.03E-17	4.92E+05	1.35E+04	2.75
29139	α Tau	Q_s	-3.058	0.029	2.06E-16	6.91E-18	2.13E+05	7.14E+03	3.36
45348	α Car	L	-1.289	0.019	1.59E-14	3.04E-16	7.83E+05	1.50E+04	1.91
45348	α Car	N	-1.309	0.020	3.38E-16	6.53E-18	1.24E+05	2.41E+03	1.94
45348	α Car	11.6	-1.307	0.025	2.17E-16	6.03E-18	9.67E+04	2.69E+03	2.78
45348	α Car	Q_s	-1.307	0.029	4.10E-17	1.37E-18	4.24E+04	1.42E+03	3.35
48915	α CMa	L	-1.360	0.017	1.70E-14	2.96E-16	8.36E+05	1.46E+04	1.75
48915	α CMa	N	-1.348	0.018	3.50E-16	6.19E-18	1.29E+05	2.28E+03	1.77
48915	α CMa	11.6	-1.346	0.023	2.24E-16	5.82E-18	1.00E+05	2.60E+03	2.59
48915	α CMa	Q_s	-1.341	0.027	4.23E-17	1.36E-18	4.38E+04	1.41E+03	3.21
81797	α Hya	L	-1.362	0.019	1.70E-14	3.19E-16	8.37E+05	1.57E+04	1.88
81797	α Hya	N	-1.309	0.019	3.38E-16	6.39E-18	1.24E+05	2.36E+03	1.89
81797	α Hya	11.6	-1.351	0.027	2.25E-16	6.59E-18	1.01E+05	2.94E+03	2.92
81797	α Hya	Q_s	-1.350	0.030	4.26E-17	1.46E-18	4.41E+04	1.51E+03	3.42
106849	ϵ Mus	L	-1.594	0.029	2.11E-14	5.83E-16	1.04E+06	2.87E+04	2.77
106849	ϵ Mus	N	-1.647	0.027	4.61E-16	1.17E-17	1.70E+05	4.32E+03	2.54
106849	ϵ Mus	11.6	-1.708	0.031	3.13E-16	1.01E-17	1.40E+05	4.53E+03	3.24
106849	ϵ Mus	Q_s	-1.700	0.039	5.89E-17	2.42E-18	6.09E+04	2.50E+03	4.10
108903	γ Cru	L	-3.299	0.039	1.01E-13	3.71E-15	4.99E+06	1.83E+05	3.66
108903	γ Cru	N	-3.354	0.038	2.22E-15	7.95E-17	8.18E+05	2.93E+04	3.58
108903	γ Cru	11.6	-3.413	0.041	1.51E-15	6.13E-17	6.73E+05	2.74E+04	4.07
108903	γ Cru	Q_s	-3.403	0.043	2.83E-16	1.27E-17	2.92E+05	1.31E+04	4.49
128620	α Cen A	L	-1.562	0.018	2.04E-14	3.58E-16	1.01E+06	1.76E+04	1.75
128620	α Cen A	N	-1.564	0.018	4.27E-16	7.57E-18	1.57E+05	2.79E+03	1.77
128620	α Cen A	11.6	-1.565	0.023	2.75E-16	7.13E-18	1.23E+05	3.18E+03	2.60
128620	α Cen A	Q_s	-1.566	0.027	5.20E-17	1.67E-18	5.38E+04	1.73E+03	3.21
133216	σ Lib	L	-1.565	0.025	2.05E-14	5.00E-16	1.01E+06	2.46E+04	2.44
133216	σ Lib	N	-1.619	0.022	4.49E-16	9.79E-18	1.66E+05	3.61E+03	2.18
133216	σ Lib	11.6	-1.680	0.028	3.05E-16	9.03E-18	1.36E+05	4.03E+03	2.96
133216	σ Lib	Q_s	-1.670	0.036	5.73E-17	2.23E-18	5.92E+04	2.30E+03	3.89
135742	β Lib	L	2.874	0.019	3.44E-16	6.39E-18	1.69E+04	3.14E+02	1.86
135742	β Lib	N	2.899	0.019	7.00E-18	1.32E-19	2.58E+03	4.85E+01	1.88
135742	β Lib	11.6	2.904	0.025	4.48E-18	1.23E-19	2.00E+03	5.49E+01	2.75

Table 9—Continued

(1)	(2)	(3)	(4)	(5)	(6)	(7)	(8)	(9)	(10)
HD	Alt.	Band	Mag	unc.	F_λ	unc.	F_ν	unc.	unc.
Name	Name	(W cm ⁻² μ m ⁻¹)	(W cm ⁻² μ m ⁻¹)	(mJy)	(mJy)	(%)
135742	β Lib	Q_s	2.915	0.029	8.40E-19	2.78E-20	8.68E+02	2.88E+01	3.32
150798	α TrA	L	-1.337	0.022	1.66E-14	3.50E-16	8.18E+05	1.72E+04	2.11
150798	α TrA	N	-1.329	0.021	3.44E-16	6.99E-18	1.27E+05	2.58E+03	2.03
150798	α TrA	11.6	-1.364	0.026	2.28E-16	6.38E-18	1.02E+05	2.85E+03	2.80
150798	α TrA	Q_s	-1.361	0.030	4.31E-17	1.48E-18	4.46E+04	1.53E+03	3.44
167618	η Sgr	L	-1.731	0.022	2.39E-14	5.08E-16	1.18E+06	2.50E+04	2.13
167618	η Sgr	N	-1.696	0.021	4.82E-16	9.86E-18	1.78E+05	3.63E+03	2.04
167618	η Sgr	11.6	-1.753	0.026	3.26E-16	9.13E-18	1.46E+05	4.08E+03	2.80
167618	η Sgr	Q_s	-1.786	0.031	6.37E-17	2.25E-18	6.59E+04	2.33E+03	3.53
216956	α PsA	L	1.002	0.019	1.93E-15	3.62E-17	9.49E+04	1.78E+03	1.88
216956	α PsA	N	1.001	0.019	4.02E-17	7.65E-19	1.48E+04	2.82E+02	1.90
216956	α PsA	11.6	1.004	0.025	2.58E-17	7.11E-19	1.15E+04	3.18E+02	2.76
216956	α PsA	Q_s	1.008	0.029	4.86E-18	1.62E-19	5.02E+03	1.67E+02	3.33

Note. — All stated quantities assume that a KRS-5 dewar window is used. If the KBr window is used, the values are nearly identical (to within 7% of the stated uncertainties).